The Journal of Neuroscience, April 1993, 13(4): 1551–1568

Immunocytochemical Localization of a Neuronal Nicotinic Receptor: The β2-Subunit

Joseph A. Hill, Jr., Michele Zoli, Jean-Pierre Bourgeois, and Jean-Pierre Changeux

URA CNRS D1284, Neurobiologie Moléculaire, Institut Pasteur, Paris 75724 Cédex 15, France

We have characterized in adult rat the tissue-specific expression of the nicotinic ACh receptor (AChR) β2-subunit using antisera raised against fusion protein constructs. Immunohistochemical localization revealed immunoreactivity distributed throughout the neuraxis. Overall, β2-like immunoreactivity (β2-LI) correlated well with *in situ* localization of β2 transcript in neuronal cell bodies. Particularly strong labeling was detected in the thalamus, and scattered other regions, whereas relatively weak staining was observed in the hypothalamus and amygdala. At the cellular level, β2-LI appeared to be exclusively neuronal and concentrated predominantly in perikarya, although strongly positive dendrites (cerebral cortical pyramidal neurons, cerebellar Purkinje cells) and axon terminals (e.g., striatum) were detected. At the ultrastructural level, β2-LI was membrane associated, with strong staining observed in endoplasmic reticulum and cytoplasmic transport vesicles. β2-LI was rarely detected at synapses. The widespread distribution of β2 suggests it may serve as a common subunit in different AChR combinations in various brain regions. Regulation of the expression of β2-subunit appears to be relatively unrestrained, with an apparent excess of protein synthesized in the cytoplasm relative to that which ultimately arrives at functional targets in the plasma membrane.

[Key words: ACh receptor, nicotinic receptor, immmunocytochemistry, CNS, rat]

Nicotinic cholinergic neurotransmission is increasingly recognized as fundamental to neuronal signaling in the mammalian CNS. ACh interacts with nicotinic receptors (AChR), leading to the opening of an intrinsic cationic channel and depolarization of the neuronal membrane. Molecular cloning methods have revealed the existence of a gene family encoding neuronal AChR subunits expressed in rat (α2, Wada et al., 1988; α3, Boulter et al., 1986; α4, Goldman et al., 1987; α5, Boulter et al., 1990; β2, Deneris et al., 1988; β3, Deneris et al., 1989; β4, Duvoisin et al., 1989; Isenberg and Meyer, 1989), chick (α2, α3, α4, and nα, Nef et al., 1988; Schoepfer et al., 1988; α7, Schoepfer et al., 1990; Couturier et al., 1990), goldfish (GFnα2, Cauley et al., 1989; GFα3 and GFnα3, Cauley et al., 1990), *Drosophila* (α-like, Bossy et al., 1988; ARD, Hermans-Borgmeyer et al., 1986; Wadsworth et al., 1988; SAD, Sawruk et al., 1990), and locust (αL1, Marshall et al., 1990) brain. Heterologous expression studies in *Xenopus* oocytes suggest that different subunit combinations assemble to form AChR pentamers (Anand et al., 1991; Cooper et al., 1991) with distinct pharmacological specificities and ionic channel properties (e.g., Luetje and Patrick, 1991, and references cited therein), implying that a wide variety of AChRs exist in the CNS and PNS.

Efficient neuronal transmission in the brain is contingent upon the geometric arrangement of presynaptic and postsynaptic elements within an elaborate circuitry. Receptor molecules are synthesized and dispatched to precise membrane domains, sometimes being transported several centimeters to plasma membrane targets. In the highly characterized model synapses of the innervated membrane of the fish electric organ and mammalian neuromuscular junction (reviewed in Changeux et al., 1990), a single type of chemical synaptic contact exists, comprising one type of receptor and one classical transmitter. In the CNS and PNS, the situation is complicated by the possible existence of several receptors and transmitters per neuron (Hökfelt, 1991). Moreover, in the case of AChR, assorted subunit combinations potentially assemble to form numerous AChR isoforms.

Thus, it is fundamental to the elucidation of nicotinic neurotransmission in the brain to identify where AChRs are located in the circuitry. Current understanding of AChR expression and distribution in the brain relies on localization of individual subunit transcripts (Wada et al., 1989, 1990; Daubas et al., 1990; Morris et al., 1990) or AChR-like immunoreactivity (using cross-reacting antibodies raised against AChR oligomers purified from heterologous species) (Deutch et al., 1987; Swanson et al., 1987; Schröder et al., 1989). These methods do not allow unambiguous localization of individual subunit proteins, and are not informative concerning AChR assembly and transport to target sites in the cell membrane. Thus, molecular probes with resolutive power at the level of individual subunit proteins are required for convincing identification and localization of AChR subunit proteins and specific AChR combinations. The cloning of cDNAs encoding functional AChR subunits has made it possible to develop such tools.

We have prepared subunit-specific antibodies in order to examine the anatomical complexities of AChR expression in the brain. In this article, we report experiments to localize AChR β2-subunit protein at tissue, cell, and ultrastructural levels in rat telencephalon, diencephalon, and cerebellum. As expected,

Received Mar. 25, 1992; revised Oct. 8, 1992; accepted Oct. 19, 1992.

This work was supported by the Centre National de la Recherche Scientifique, the Collège de France, the Institut National de la Santé et de la Recherche Médicale (Contract 872004), and the Direction des Recherches et Etudes Techniques (Contract 87/211). Support from postdoctoral fellowships awarded by the National Institutes of Health (J.A.H.) and the European Molecular Biology Organization (M.Z.) is acknowledged. We are grateful to Drs. Alain Bessis and Philippe Daubas for critical reading of the manuscript.

Correspondence should be addressed to Dr. Jean-Pierre Changeux, Neurobiologie Moléculaire, Institut Pasteur, 25 Rue du Docteur Roux, 75724 Paris Cédex 15, France.

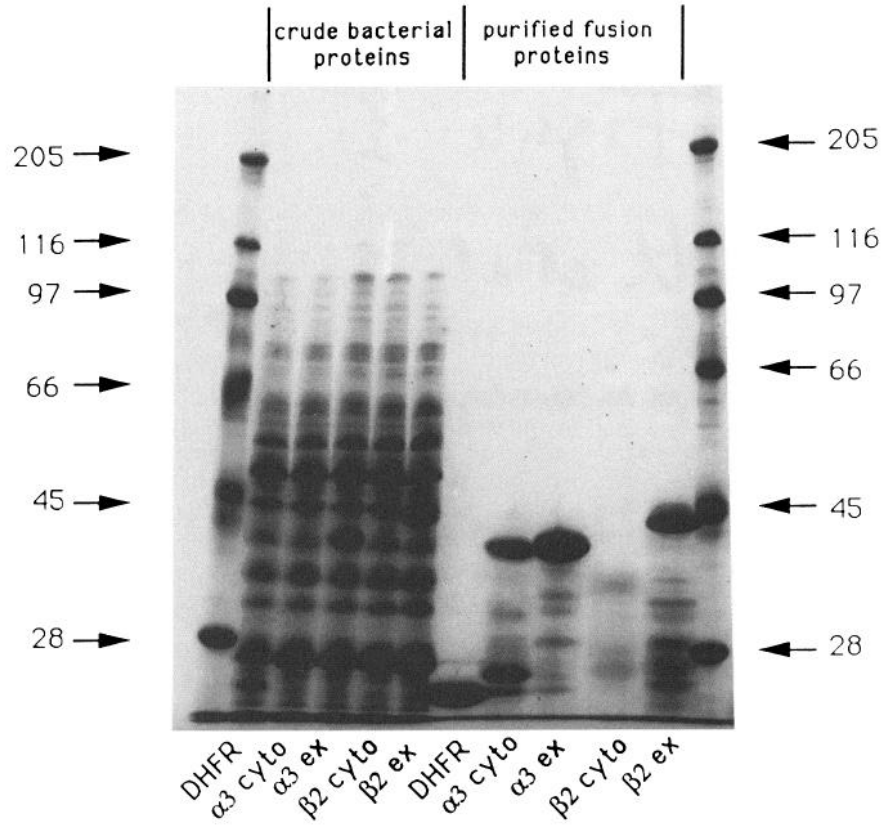

Figure 1. Recombinant AChR subunit proteins expressed in *E. coli*. Fusion proteins were engineered containing extracellular and cytoplasmic domains specific for rat β2 (see text for details) and α3 (Hill, Zoli, Bourgeois, and Changeux, unpublished observations) subunits. Crude protein extracts of induced *E. coli* cultures are in *lanes 2–6*; fusion proteins purified by nickel chelate affinity chromatography are in *lanes 7–11*.

β2-like immunoreactivity (β2-LI) was widely distributed, though largely restricted to cholinergic regions of the brain. The distribution of cell bodies expressing β2-LI correlated well with the localization of β2 gene expression as observed by *in situ* hybridization (ISH); evidence for the transport of β2 protein was inferred from those instances where transcript and protein localization differed. β2-LI was strictly membrane associated, with a conspicuous predominance of staining of intracellular membranes relative to those at the cell surface.

Materials and Methods

Fusion protein constructs

Two β2 fusion protein constructs were engineered using standard DNA cloning techniques (Sambrook et al., 1989): (1) the hydrophilic sequence (123 amino acids) between membrane-spanning domains M3 and M4 (β2 cytoplasmic), and (2) the N-terminal region (176 amino acids) (β2 extracellular) of rat β2-subunit. In each case, a fusion protein consisting of the β2 sequence of interest fused C-terminal to a derivative of mouse dihydrofolate reductase (DHFR) was engineered (plasmids generously provided by Dr. Dietrich Stüber, Hoffman-LaRoche, Basel; currently commercialized by Qiagen). A means of purification by chelate affinity chromatography was provided by a histidine hexamer N-terminal to dihydrofolate reductase (Stüber et al., 1990).

β2 cytoplasmic. A 369 base pair (bp) fragment (nucleotides 999–1368 of Deneris et al., 1988) was obtained by NcoI digestion of β2 rat cDNA (pCX49, kindly provided by Dr. Steven Heinemann) and rendered blunt-ended using Klenow fragment DNA polymerase. A pDS781/RBSII,6xHis-DHFR expression vector was digested with BglII and rendered blunt-ended using Klenow fragment DNA polymerase. The DNA fragment was subcloned and conservation of the reading frame across the fused junction was confirmed by dideoxy sequencing (Pharmacia). The sequence of the β2 cytoplasmic loop component of the resulting fusion protein was: APWVKVVFLEKLPTLLFLQQPRHRCARQRLR LRRRQREREGEAVFFREGPAADPCTCFVNPASVQGLAGAFRAE PTAAGPGRSVGPCSCGLREAVDGVRFIADHMRSEDDDQSVRED WKYVA. This sequence was chosen as it is unique to and specific for β2-subunit protein. Cross-reactivity with other known AChR subunits is very unlikely as alignment calculations (not shown) established that no stretches of identical amino acids exist that are long enough (>4 amino acids) to constitute an antibody epitope.

β2 extracellular. A fusion protein construct was engineered for the N-terminal domain of β2. Although the amino acid sequence in this region of the protein is less specific for β2, antisera directed against the N-terminus served as useful controls for the specificity of β2-LI staining pattern; though cross-reactivity with other AChR subunits might be expected, immunostaining with β2 extracellular antisera defines an outer limit to the true distribution of β2-subunit.

A 530 bp fragment (nucleotides 121–651 of Deneris et al., 1988) was obtained from BstYI and HgaI digestion of pCX49 and rendered blunt-ended using Klenow fragment DNA polymerase. A pDS781/RBSII,6xHis-DHFR(-2) expression vector was digested with BglII and rendered blunt-ended using Klenow fragment DNA polymerase. The DNA fragment was subcloned and conservation of the reading frame across the fused junction was confirmed by DNA sequencing. The sequence of the β2 extracellular domain component of the resulting fusion protein was: DPSRYNKLIRPATNGSELVTVQLMVSLAQLISVHER EQIMTTNVWLTQEWEDYRLTWKPEDFDNMKKVRLPSKHIWL PDVVLYNNADGMYEVSFYSNAVVSYDGSIFWLPPAIYKSACKIE VKHFPFDQQNCTMKFRSWTYDRTEIDLVLKSDVASLDDFTPSG EWDIIALPGRRN.

Preparation of fusion proteins and generation of antibodies

Expression plasmids were transformed into *Escherichia coli* SG13009 cells (Gottesmann et al., 1981) harboring a repressor plasmid (pUHA1) carrying *neo* and *lacI* genes. Recombinant proteins were induced and purified by nickel chelate affinity chromatography according to Stüber et al. (1990) (Fig. 1). Polyclonal antisera were raised in adult male New Zealand rabbits by a hyperimmunization protocol: ≈250 μg of recombinant protein was emulsified in adjuvant (Freund's complete for first injection, Freund's incomplete thereafter) and injected subcutaneously (10–12 sites) four times at 6 week intervals.

In all experiments, β2 antisera were preadsorbed with rat dihydrofolate reductase (DHFR). In addition, antisera were routinely conditioned by preadsorption with rat brain acetone powder and innervated

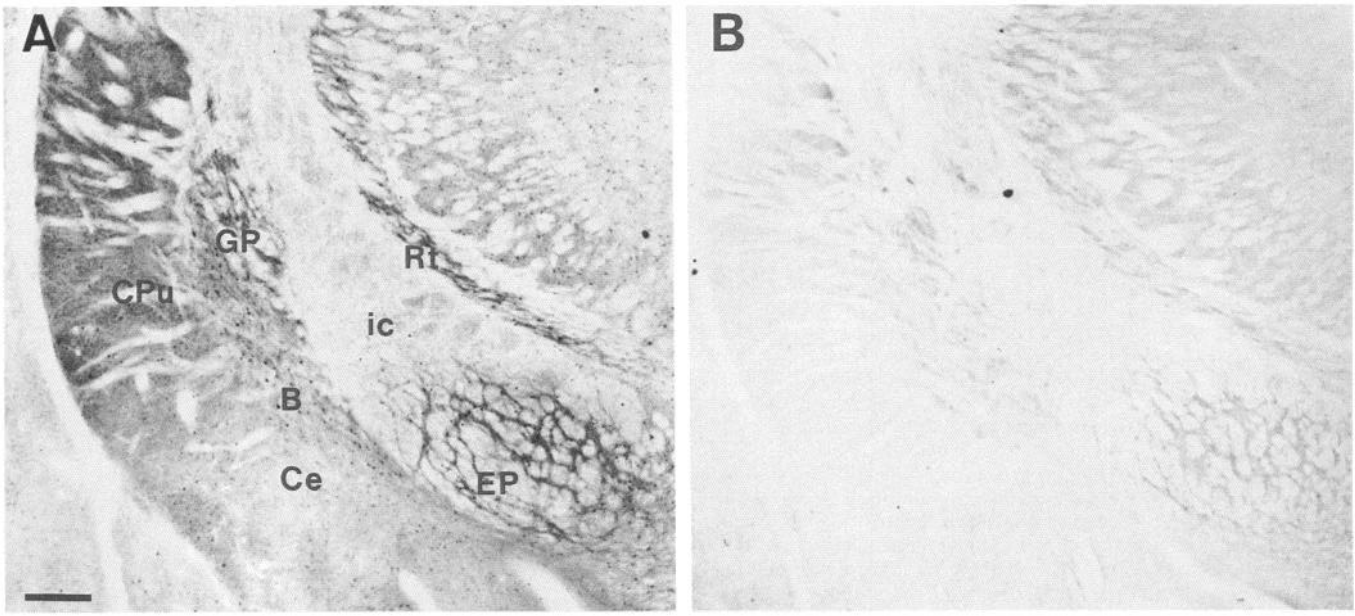

Figure 2. Photomicrographs of rat basal ganglia and ventrolateral thalamus stained with immune (*A*, Ab170) and preimmune (*B*) antisera against fusion protein containing the cytoplasmic domain of rat β2. *Ce*, central amygdaloid nucleus; *CPu*, caudate-putamen; *B*, basal nucleus of Meynert; *EP*, entopeduncular nucleus; *GP*, globus pallidus; *ic*, internal capsule; *Rt*, reticular thalamic nucleus. Level = bregma −2.8 mm; antibodies diluted 1:1000, revealed by DAB/Ni. Scale bar, 400 μm.

membranes from *Torpedo* electrocyte (to eliminate cross-reactivities stemming from epitopes shared with peripheral AChR; prepared according to Hill et al., 1991). Experiments performed using preimmune sera (derived from the same animal) (Fig. 2) or with anti-β2 antibodies after preadsorption with excess of the appropriate fusion protein (Fig. 3) yielded an absence of the specific pattern of staining.

Immunoblots of recombinant protein or adult rat cortical membranes were probed with Ab170 (anti-β2 cytoplasmic fusion protein) and revealed the presence of specific bands (data not shown). Preadsorption with recombinant protein led to a dramatic diminution in the intensity of these bands. In the case of crude protein from adult cortex, a strong, preadsorbable band was detected at ≈40 kDa, in the approximate range where immunopurified β2-subunit is found (Whiting and Lindstrom, 1987). In addition, a second, faster migrating band was seen at ≈28 kDa. We interpret the band at ≈40 kDa to be native β2-subunit protein and the faster band to be a product of proteolytic degradation.

Anti-peptide antibodies

To provide additional anatomical controls, polyclonal antisera were raised against synthetic peptides specific for extracellular (DTEERLVE HLLDPSRY) and intracellular (RQRLRLRRRQREREGEY) domains of β2. Synthetic peptides were coupled to keyhole limpet hemocyanin (molar ratio of 2000:1) using a bis-diazotized benzidine procedure (Harlow and Lane, 1988). Rabbits were immunized as above. Preimmune sera or sera preadsorbed with synthetic peptide (50 μg of peptide per milliliter of diluted serum) failed to stain tissue sections.

Affinity purification of antibodies

β2-cytoplasmic fusion protein was covalently coupled to beads (Affi-Gel 10, Bio-Rad) and incubated overnight with antiserum. After thorough washing, specific antibodies were eluted first in acid (pH 2.5) and then base (pH 11.5). Fractions were pooled and concentrated by ultrafiltration (Centricon).

Immunocytochemical procedures and optic microscopy

Sprague–Dawley rats (150–200 gm body weight) were killed under deep chloral hydrate anesthesia (35%, 2 ml/kg, i.p.) by intracardiac perfusion with 100 ml of saline followed by 100/150 ml of ice-cold 2% paraformaldehyde, 0.2% picric acid in 0.1 M phosphate buffer (pH 7.2). The

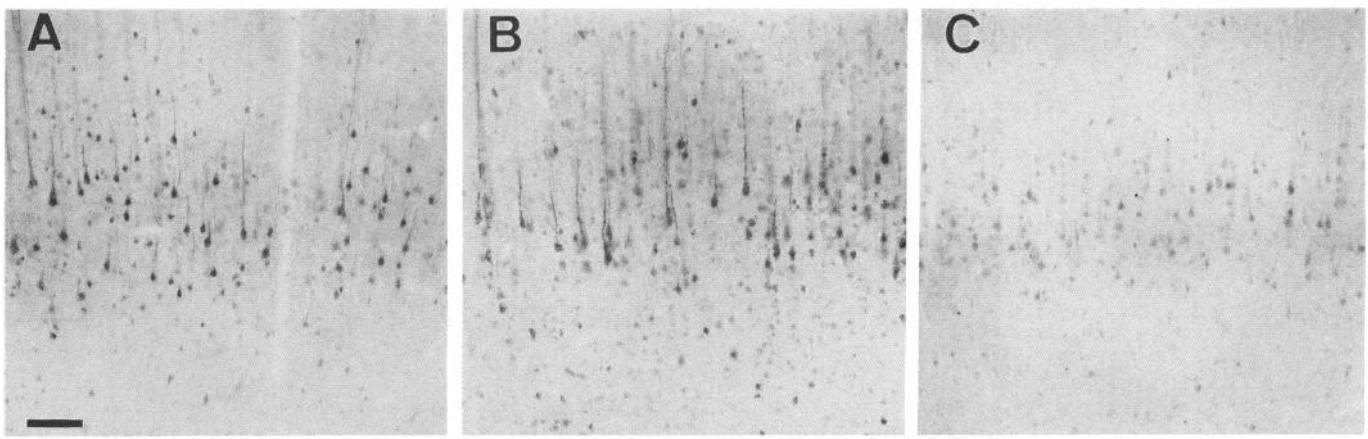

Figure 3. Photomicrographs of layer V of rat cerebral cortex stained with antibodies against fusion protein containing the cytoplasmic (*A*, Ab170) or extracellular (*B*, Ab167) domains of rat β2. *C* shows an adjacent section stained with Ab170 preadsorbed with β2 cytoplasmic fusion protein. Level = bregma −2.2 mm; antibodies diluted 1:500, revealed by DAB. Scale bar, 100 μm;

brains were rapidly dissected out and postfixed for 30 min in the same fixative. Similar results were obtained with 100 ml of 3% paraformaldehyde, 0.2% picric acid or with 300 ml of 2–3% paraformaldehyde. Four percent paraformaldehyde with or without picric acid as well as postfixation times longer than 2–4 hr resulted in a marked decrease in staining intensity. Brains were cryoprotected by incubation in first 15% and then 30% sucrose (0.1 M phosphate buffer) over 2 d (4°C). The brains were cut on a cryotome (50-μm-thick sections) or vibratome (50–60-μm-thick sections).

Before incubation with primary antibody, free-floating sections were incubated 30 min at room temperature (RT) in blocking buffer [phosphate buffered saline (PBS; pH 7.2) containing 1% bovine serum albumin (BSA), 0.1% gelatin, and 5% normal serum (NS)]. Sections were incubated overnight at 4°C in primary antibody diluted in incubation buffer (PBS containing 1% BSA, 0.1% gelatin, and 1% NS). Antibody dilutions ranged from 1:100 to 1:5000. Optimal results were obtained at 1:500 when using streptavidin peroxidase or streptavidin-gold as detection systems, 1:1000 when using peroxidase detection plus nickel intensification.

Sections were rinsed 3 × 15 min in washing buffer (PBS containing 1% BSA and 0.1% gelatin) and incubated with the secondary antibody (biotinylated anti-rabbit; Amersham; dilution, 1:200) in incubation buffer for 1 hr at RT. After three 10 min rinses in washing buffer, the sections were incubated in streptavidin–biotinylated peroxidase preformed complex (Amersham; 1:100) or streptavidin–gold (1 nm diameter; Amersham; 1:50) for 30 min or 4 hr, respectively, at RT. In the case of peroxidase detection, 3,3′-diaminobenzidine (DAB) (0.05% in 0.05 M Tris-HCl, pH 7.2) plus 0.016% H_2O_2 with or without ammonium nickel sulfate (0.07%) was used as chromogen. Detection of gold particles (1 nm) was enhanced using silver amplification (Amersham). Anatomical nomenclature used in this report follows that of Paxinos and Watson (1982).

Electron microscopy

Vibratome sections (80 μm) were incubated (overnight at 4°C) in primary antiserum and processed as above for peroxidase or gold labeling. Blocks of tissue were dehydrated in stepped ethanols and flat embedded in epoxy resin. As antibody penetration was limited in the vibratome sections (in absence of detergent), labeling was largely confined to a few micrometers under the surface of the blocks. Ultrathin sections were examined using a Philips CM 12 electron microscope without counterstaining.

In situ *hybridization*

In situ hybridization (ISH) was performed on cryostat sections (14 μm) as described previously (Young, 1990). Probes were 3′ end-labeled with ^{35}S-dATP using terminal deoxynucleotidyl transferase (Boehringer-Mannheim). Four nonoverlapping antisense oligonucleotides from the putative cytoplasmic domain of β2 between membrane-spanning segments M3 and M4 gave the same pattern of hybridization: AGCCAA GCCCTGCACTGATGCAGGGTTGACAAAGCAGGTACATGG, TCGCATGTGGTCCGCAATGAAGCGTACGCCATCCACTGCTTC CCG, TGACAAAGCAGGTACATGGGTCAGCCGCAGGACCTTC ACGGAAGA, TCGCCCTCACGCTCTCGCTGGCGCCTCCTCAAG CGCAGA. Specificity was additionally assured by the absence of labeling above background in experiments with oligonucleotides of the same GC content and length but unrelated sequences.

Results

Specificity of β2-LI localization

Incubation of tissue sections with β2 antisera generated reproducible patterns of staining within discrete populations of neurons and neuronal processes. To assess the specificity of the antibody staining, several anatomical control experiments were performed in addition to the routine immunohistochemical controls (absence of staining with preimmune sera or after antigen preadsorption; see Materials and Methods).

The same staining pattern was observed with all anti-β2 antibodies tested. Criteria for similarity were defined as staining patterns identical in terms of neuronal types and their localization throughout several brain regions; all control experiments (see below) met these criteria for similarity and allowed us unambiguously to define the distribution of β2-LI. Differences in immunolabeling that were observed exclusively involved relative intensities of somatic versus terminal field staining and differences in general background levels.

First, the same staining pattern was observed whether the antibodies were directed against a cytoplasmic domain or an extracellular domain of β2 (Fig. 3). Second, antisera directed against fusion proteins and against synthetic peptides provided the same β2-LI staining patterns, even if antibodies against synthetic peptides showed a lower staining intensity. Third, for each antigen construct, antisera were raised in at least three rabbits, and sera prepared from each animal provided the same β2-LI staining patterns. Fourth, anti-β2 cytoplasmic fusion protein polyclonal antisera purified on an antigen column produced the same β2-LI staining pattern. Fifth, the regional distribution of cell bodies with β2-LI was found to be in good agreement with that of β2 mRNA as visualized by ISH (Figs. 4, 5; see below for a detailed description). Sixth, the regional distribution of β2-LI was found to be dissimilar from those of β4, α3, and α4 mRNAs as visualized by ISH. For this control the hippocampal area and medial habenula were chosen as these regions contain a unique distribution of the four mRNAs considered. As shown in Figure 4, in the pyramidal layer of the hippocampus only β2 mRNA is expressed, whereas in the medial habenula the four mRNAs are expressed but differently localized in the nucleus. In fact, β4 and α3 mRNAs are strongly expressed only in the ventral part of the medial habenula, α4 mRNA is more expressed in the lateral part of the medial habenula, and β2 mRNA is homogeneously but weakly expressed in the entire medial habenula. As shown in Figure 5, the β2-LI cell body distribution specifically corresponds to the β2 mRNA pattern (see also Fig. 12). Taken together with the observations from preadsorption and preimmune serum experiments, these data indicate that the β2-LI staining pattern was specific. After establishing the specificity of the labeling pattern, we performed the majority of experiments with antiserum 170 (anti-β2 cytoplasmic fusion protein).

Regional distribution of β2-LI

Olfactory regions. Rat olfactory bulb showed a very heterogeneous laminar distribution of β2-LI (Fig. 6*A*). Most mitral cell bodies were intensely stained, and in the periglomerular layer moderately stained cell bodies and long neuronal processes were present. In the other layers only occasional weakly stained cell bodies could be detected. The anterior olfactory nucleus (Fig.

→

Figure 4. Dark-field images of emulsion autoradiograms of β2 (*A*, *E*), β4 (*B*, *F*), α3 (*C*, *G*), and α4 (*D*, *H*) ISH in rat dorsomedial thalamic and hippocampal regions. *E–H* represent higher magnifications of medial habenula regions shown in *A–D*. Antisense oligonucleotides: β2 = TGACA AAGCAGGTACATGGGTCAGCCGCAGGACCTTCACGGAAGA; β4 = AGCTGACACCCTCTAATGCTTCCTGTAGATCTTCCCGGAACC TCC; α3 = CCCAAGTGGGCATGGTGTGTGTGGTTGGAGTTCTATAGTGCAC; α4 = GCTGCTTCTTGGGAGCTGGGCACATGCTGGA CACTCAGGGACCTG. *Broken lines* delimit the medial habenula; *arrows* indicate the pyramidal layer of CA1 field. Level = bregma −3.8 mm. Scale bars: *A–D*, 250 μm; *E–H*, 100 μm.

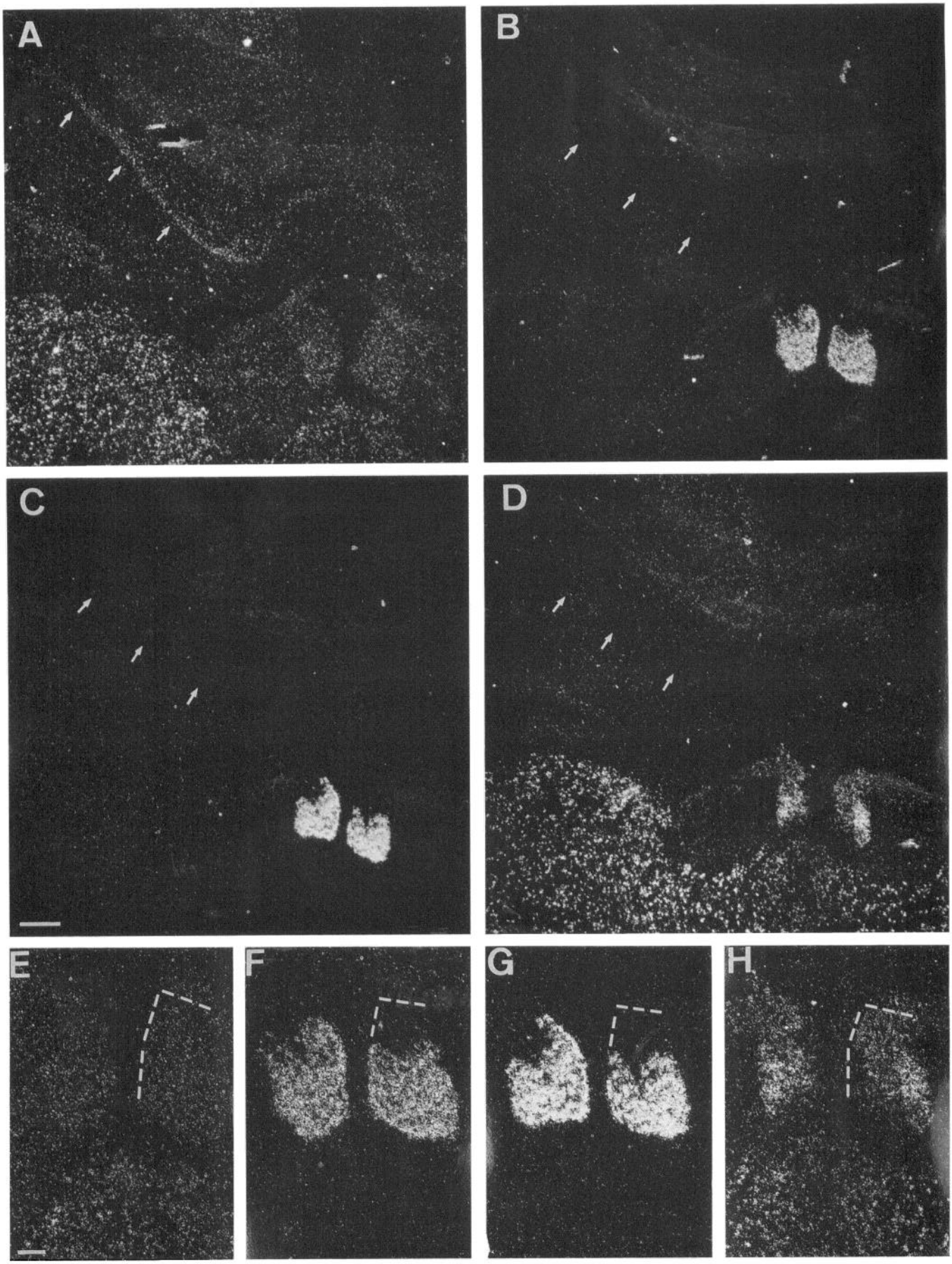
A
B
C
D
E
F
G
H

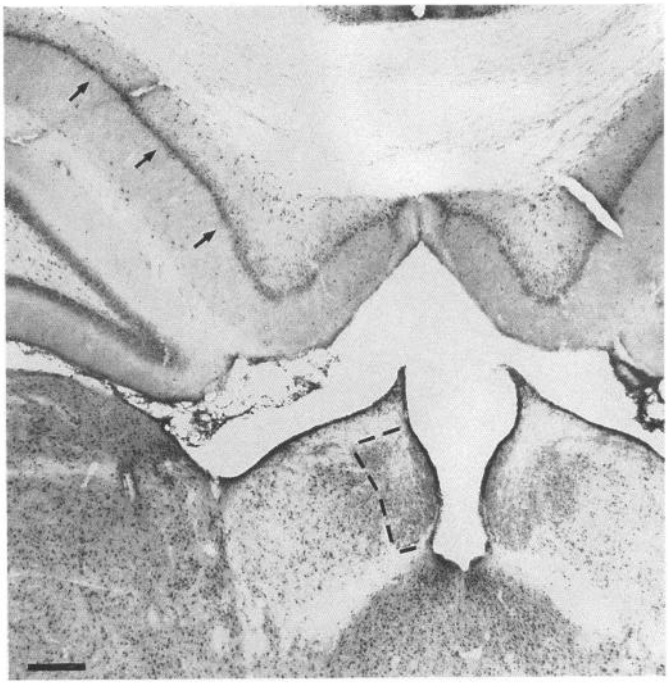

Figure 5. Photomicrograph of β2-LI in rat dorsomedial thalamic and hippocampal regions. *Broken line* delimits the medial habenula; *arrows* indicate the pyramidal layer of CA1 field. Level = bregma −3.8 mm; Ab170 diluted 1:1000, revealed by DAB/Ni. Scale bar, 250 μm.

6*B*) contained a large number of moderately to intensely stained neurons. Olfactory tubercle (Fig. 7*A*) and piriform cortex (Fig. 7*B*) showed a similar pattern of staining, that is, layer II highly stained, layer III moderately stained, and the outer layer I almost unstained. All densely packed neurons of layer II appeared to be positive.

Isocortex. In the isocortex, distinct heterogeneity in the laminar distribution of β2-LI was present (Fig. 8*A*). The most prominent staining was observed in the large pyramidal neurons of layer V, which showed strongly labeled cell bodies and apical dendrites; in contrast, the lateral dendrites were only inconstantly visualized. A moderate number of positive cell bodies were present in cortical layers II/III, and a few neurons in layer VI were stained. Cortical layers I and IV were almost devoid of staining.

Hippocampal formation. In the hippocampus, most pyramidal and granular cell bodies and many apical dendrites were weakly to moderately stained (Fig. 8*B*; see also Figs. 5, 12). This pattern was similarly observed in subregions CA1–CA3 and dentate gyrus. The most prominent staining, however, was observed in sparsely distributed interneurons in all layers, including the pyramidal layer, where they were intermingled with pyramidal neurons. In the hilar regions of the dentate gyrus, several large polymorph cells were intensely stained. In all subiculum and entorhinal cortex subregions, most of the densely packed cells of layer II were positive together with scattered cells in internal layers. The cell labeling in layer II exhibited a gradient in intensity across the various hippocampal subregions (Table 1). For instance, in entorhinal cortex a gradient toward decreased staining intensity was observed moving from the lateral to the medial part.

Basal ganglia. In both dorsal and ventral striatum, sparsely distributed large neurons (possibly corresponding to cholinergic cells) were intensely stained whereas weaker labeling was observed in many medium-sized neurons (Fig. 9*B*). The entire striatal region appeared to be extremely rich in delicate neuronal processes, giving the impression of elevated background to this area (Fig. 2). A continuous band of intensely stained neurons with an elaborate dendritic arborization was localized in globus pallidus and substantia innominata (Fig. 9*B*), again surrounded by dense, fine neuropil staining. Many moderate to intensely immunoreactive neurons and dense neuropil staining were also observed in the subthalamic (Fig. 9*A*) and entopeduncular (Fig.

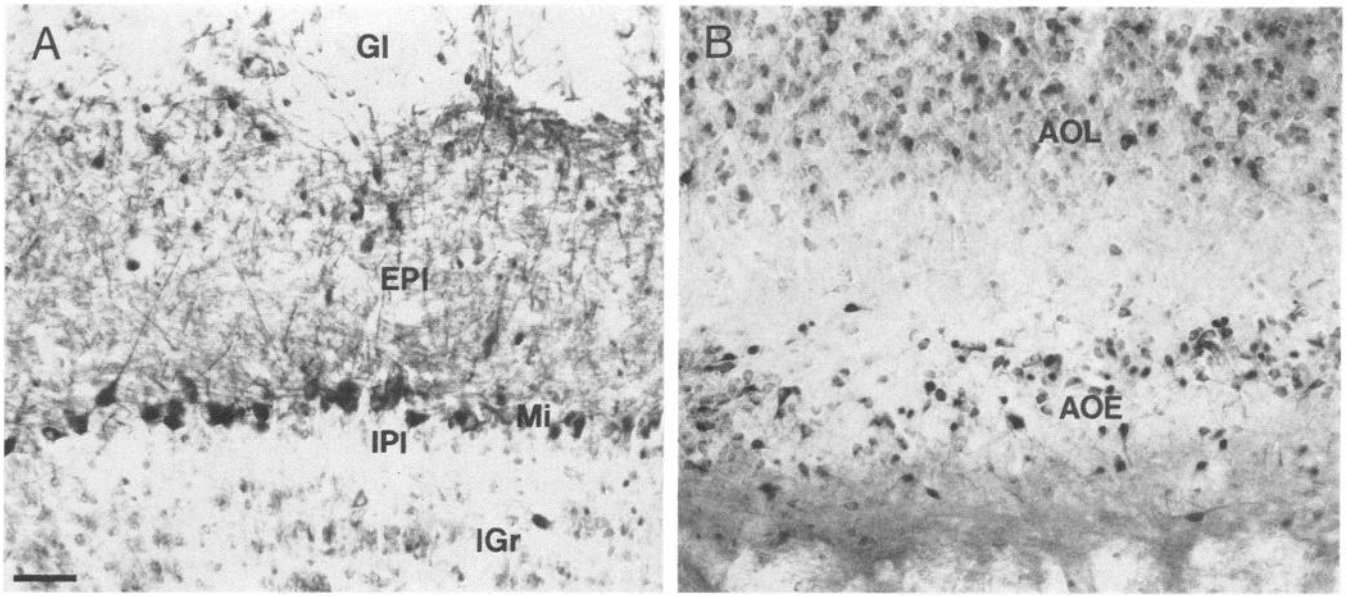

Figure 6. Photomicrographs of β2-LI in rat olfactory regions. *A*, Olfactory bulb. *Gl*, glomerular layer; *EPl*, external plexiform layer; *IPl*, internal plexiform layer; *IGr*, internal granular layer; *Mi*, mitral cell layer. *B*, Anterior olfactory nuclei. *AOL*, anterior olfactory nucleus, lateral part; *AOE*, anterior olfactory nucleus, external part. Level = bregma 5.7 mm; Ab170 diluted 1:1000, revealed by DAB/Ni. Scale bar, 50 μm.

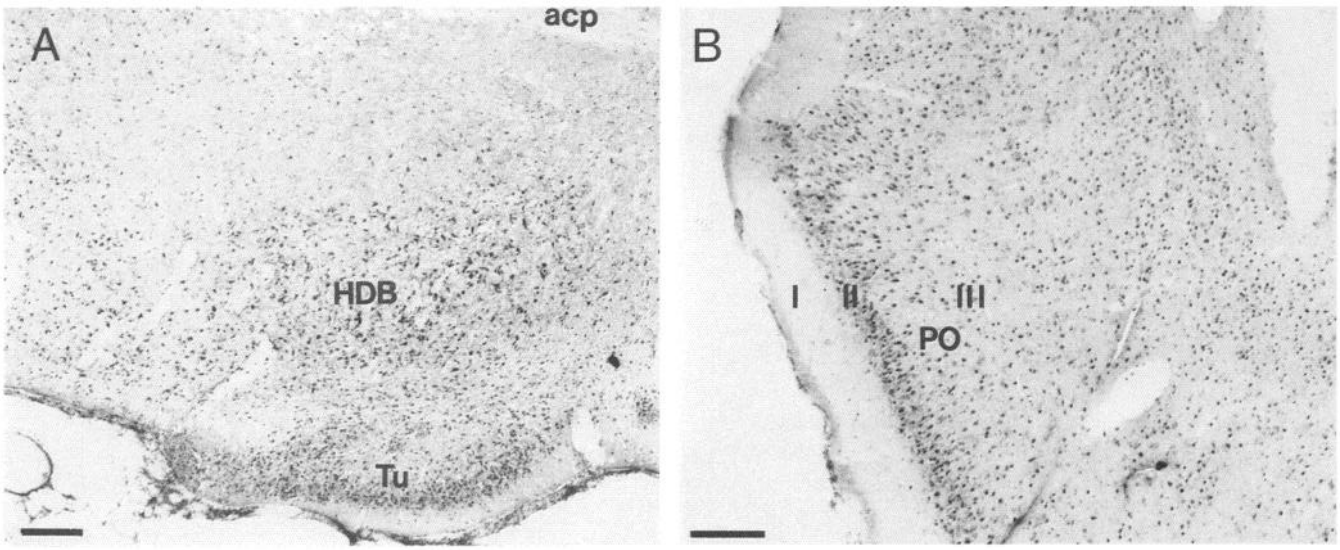

Figure 7. Photomicrographs of β2-LI in rat olfactory regions. *A*, Olfactory tubercle and adjacent regions. *acp*, anterior commissure, posterior part; *HDB*, nucleus of the horizontal limb of the diagonal band; *Tu*, olfactory tubercle. Level = bregma −0.3 mm. *B*, Olfactory cortex. *PO*, Primary olfactory cortex, layers *I–III*. Level = bregma −4.3 mm; Ab170 diluted 1:1000; revealed by DAB/Ni. Scale bars, 200 μm.

2) nuclei. In the ventral mesencephalon, most neurons as well as neuropil of the pars compacta and reticulata of the substantia nigra and the ventral tegmental area appeared to be moderately to intensely stained (Fig. 9*C*).

Septum and limbic forebrain. The septal area contained several distinct clusters of intermediate to intensely stained neurons (Fig. 10). In particular, in the dorsal part of lateral septum many moderately stained cells were observed (Fig. 10*B*), and in the median septum most cells were moderately to intensely stained (Fig. 10*A*). These positive cells extended to the nucleus of the vertical limb of the diagonal band and, at more caudal levels, to the nucleus of the horizontal limb of the diagonal band (Fig. 7*A*). As in the striatum, these cells exhibited distinct and rich dendritic arborization. Several other nuclei, such as the bed nucleus of the stria terminalis and septofimbrial and triangular septal nuclei, were weakly to moderately stained. Among them, the bed nucleus of anterior commissure was exceptional in that dense neuropil staining was also present.

Amygdala. Overall, the amygdaloid region was relatively poorly stained (Fig. 2). However, many moderately stained cell bodies were present in cortical and, to a lesser extent, medial amygdala. Occasional intensely stained cells were detected in the basolateral amygdala. Weakly stained cells were rarely observed in the other subregions.

Thalamus. The thalamus exhibited the highest overall β2-LI in rat brain (Figs. 11*B,D*; 12). Indeed, ventral group thalamic nuclei manifested the most intense staining observed in the adult CNS. Overall, however, the thalamic staining pattern was rather heterogeneous among different subregions (Fig. 12). The highest degree of cell body labeling was observed in the ventral nuclei and in the posterior complex. Somewhat lower labeling was observed in anterior (Fig. 11*B*), lateral, and mediodorsal groups of nuclei, and relatively weak but specific labeling was seen in midline nuclei. In each of the thalamic nuclei, most neurons appeared to be stained (Fig. 11*D*).

Intralaminar nuclei appeared to be both relatively weakly and more sparsely stained, with the exception of the parafascicular nucleus, which was intensely stained. Scant cells of the reticular nucleus and zona incerta were intensely stained (Fig. 11*B*). In the habenular complex, all clustered cells of the medial habenula appeared weakly stained, whereas fewer cells were positive in the lateral habenula (Figs. 5, 12). Many cells were strongly stained in the medial geniculate nucleus and in the dorsal part of the lateral geniculate, while a sparser and less intense staining was observed in the ventral lateral geniculate. Densely stained neuropil was apparent in the ventral posterior nuclei, the lateral geniculate (especially the dorsal part), in the reticular nucleus and the zona incerta.

Hypothalamus. Overall, the hypothalamus was relatively poor in β2-LI relative to the thalamus. A relatively intense labeling was, however, observed in magnocellular nuclei (paraventricular hypothalamic and supraoptic nuclei and accessory ones), the preoptic area, and mammillary nuclei (in particular, the supramammillary and lateral mammillary nuclei; see Fig. 13). Moderate staining was also observed in the suprachiasmatic, ventrolateral, and arcuate nuclei, and in the retrochiasmatic and lateral hypothalamic areas.

Cerebellum. In the cerebellum, staining was mostly restricted to Purkinje cells and dendrites (Fig. 14*B*). Weakly stained granular cells were also observed (Fig. 14*D*). Several neurons in the deep cerebellar nuclei were moderately stained.

In situ *hybridization studies*

We have localized β2 transcript in selected regions of the brain in order to compare β2 gene expression with the distribution of β2-LI. We carried out ISH histochemistry using oligonucleotide probes from specific portions of the β2 mRNA (see Materials and Methods). Overall, we observed substantial correlation between β2-LI immunolabeling in neuronal somata and *in situ* localization of β2 transcript.

For example, in the hippocampus, localization of β2 transcript to pyramidal cells and interneurons matched exactly with the presence of β2-LI in these same cells (Figs. 4, 5, 11*A*, 12). In thalamus, β2 transcript accumulated to high levels and was widely distributed (Fig. 11*A*). At higher magnification, practically all neurons in the ventroposterior part of the thalamus were positive for β2 mRNA (Fig. 11*C*), a pattern similar to that of β2-LI (Fig. 11*D*). In cerebellum, a strong signal was detected

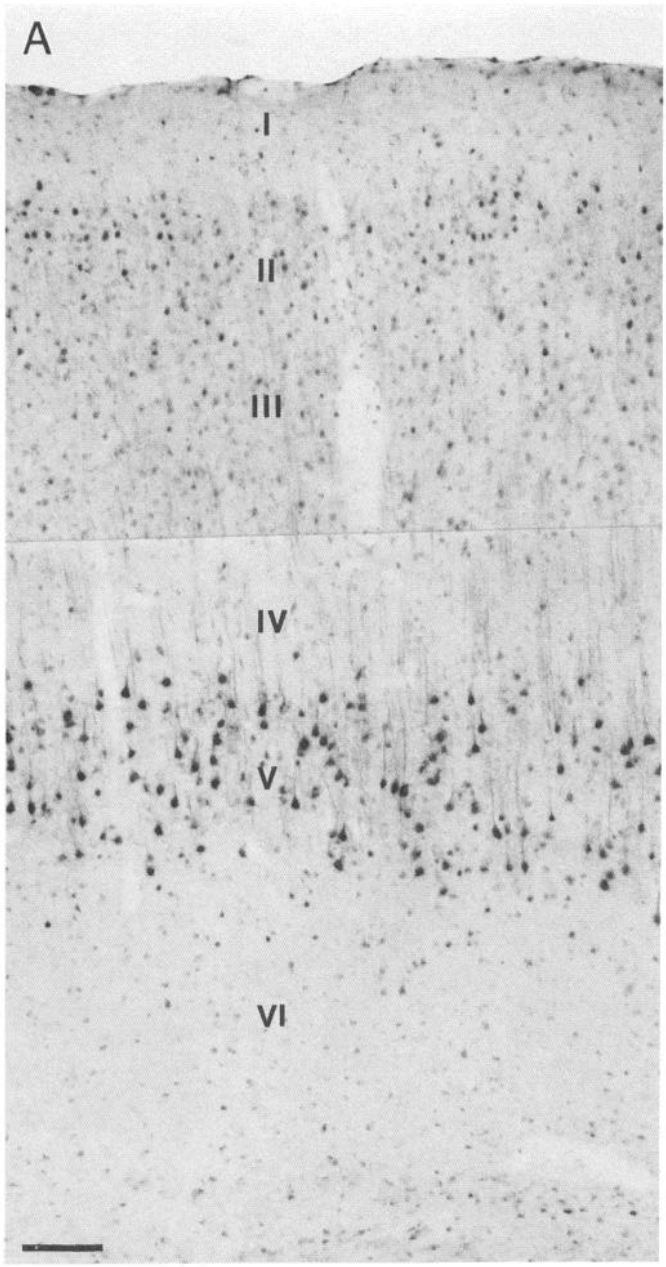

Table 1. β2-LI in telencephalon, diencephalon, and cerebellum

Brain regions	Density[a]	Intensity[b]
A. Isocortex		
I	1	a
II	2	b
III	1.5	ab
IV	1	a
V	2.5	bc
VI	1.5	ab
Claustrum	1.5	b
B. Olfactory regions		
1. Main bulb		
Periglomerular layer	1	a
Outer plexiform layer	2	ab
Mitral layer	3	b
Inner plexiform layer	1	a
Granular layer	1	a
2. Anterior olfactory n.		
Lateral part	3	ab
External part	2	bc
3. Olfactory tubercle		
I	1	a
II	3	b
III	1.5	ab
4. Piriform cortex		
I	1	a
II	3	b
III	1.5	ab
Endopiriform cortex	2	b
C. Hippocampal formation		
1. Entorhinal area (lateral)		
I	1	a
II	3	bc
III	1	a
IV–VI	2	ab
Entorhinal area (medial)		
I	1	a
II	3	ab
III	1	a
IV–VI	2	ab
2. Subiculum		
Molecular layer	1	bc
Stratum radiatum	1	bc
Pyramidal layer	3	ab
3. CA1		
Stratum lacunosum-moleculare	1	bc
Stratum radiatum	1	bc
Pyramidal layer	3	ab
Stratum oriens	1	bc

←

Figure 8. Photomicrographs of β2-LI in rat cerebral cortex and hippocampus. *A*, Frontoparietal cortex, layers I–VI. Level = bregma −2.8 mm; Ab170 diluted 1:1000; revealed by DAB/Ni. *B*, Hippocampal field CA1. *lm*, Stratum lacunosum-moleculare; *or*, stratum oriens; *py*, stratum pyramidale; *ra*, stratum radiatum. The photograph was intentionally overexposed to reveal dendritic field details, which explains the high intensity of staining in pyramidal cells compared to Figures 5 and 12. Level = bregma −4.3 mm; Ab170 diluted 1:500; revealed by DAB/Ni. Scale bars: *A*, 100 μm; *B*, 50 μm.

Table 1. Continued

Brain regions	Density[a]	Intensity[b]
4. CA3		
Stratum lacunosum-moleculare	1	bc
Stratum radiatum	1	bc
Pyramidal layer	3	ab
Stratum oriens	1	bc
5. Dentate gyrus		
Molecular layer	1	bc
Granular layer	3	ab
Polymorph layer	2	bc
D. Amygdala		
1. Medial nucleus	2	ab
2. Cortical nucleus	3	b
3. Central nucleus	1.5	a
4. Lateral nucleus	1	b
5. Basolateral nucleus	1.5	bc
6. Basomedial nucleus	1.5	ab
7. Intercalated nuclei	1	a
E. Septum		
1. Lateral nucleus		
Dorsal part	2	b
Intermediate part	1	a
Ventral part	1	a
2. Medial nucleus	2.5	bc
3. Nucleus of the diagonal band		
Vertical limb	2.5	bc
Horizontal limb	2.5	bc
4. Bed n. stria terminalis	1.5	ab
5. Bed n. anterior commissure	2	ab
6. Septofimbrial nucleus	2	ab
7. Triangular nucleus	2	a
8. Septohippocampal n.	2	ab
F. Basal ganglia		
1. Striatum: large cells	1	bc
2. Striatum: medium-sized cells	2	ab
3. Globus pallidus	2	c
4. Entopeduncular n.	2	b
5. Substantia innominata	2	c
6. Subthalamic n.	2	bc
7. Substantia nigra		
Pars compacta	3	bc
Pars recticulata	2	bc
8. Ventral tegmental area	3	bc
G. Thalamus		
1. Medial habenula	3	a
2. Lateral habenula	1.5	ab
3. Anterior group		
Anteroventral n.	2	b
Anterodorsal n.	2	b
4. Mediodorsal n.	3	b
5. Lateral group		
Lateral dorsal n.	3	b
Lateral posterior n.	3	bc
6. Midline group		
Paraventricular n.	2	ab
Parataenial n.	2	b
N. reuniens	3	ab
Rhomboid n.	3	ab
N. gelatinosus	3	bc

Table 1. Continued

Brain regions	Density[a]	Intensity[b]
7. Ventral group		
Ventral anterior/ventral lateral	3	c
Ventral medial	3	c
Ventral posterior	3	c
8. Posterior complex	3	c
9. Medial geniculate n.	3	bc
10. Lateral geniculate n.		
Dorsal part	3	c
Ventral part	2	b
11. Intralaminar nuclei		
Central medial n.	2	ab
Paracentral n.	2	ab
Central lateral n.,	2	ab
Parafascicular n.	3	bc
12. Reticular n.	2.5	bc
13. Zona incerta	2	b
14. N. fields of Forel	1.5	ab
H. Hypothalamus		
1. Paraventricular zone		
Preoptic periventricular n.	1	ab
Suprachiasmatic n.	2	b
Supraoptic n.	2	bc
Paraventricular n.		
Parvicellular part	1.5	ab
Magnocellular part	2	bc
Anterior periventricular n.	1	ab
Arcuate n.	2	ab
2. Medial zone		
Medial preoptic area	2	b
Anterior hypothalamic n.	1.5	ab
Retrochiasmatic area	2	b
Ventromedial n.	2	b
Dorsomedial n.	1	ab
Premammillary n.	2	b
Supramammillary n.	2.5	bc
Lateral mammillary n.	2	bc
Medial mammillary n.	2.5	ab
3. Lateral zone		
Lateral preoptic area	1.5	b
Lateral hypothalamic area	2	b
Posthypothalamic area	1.5	b
I. Cerebellum		
1. Deep nuclei	2	bc
2. Cortex		
Molecular layer	1	a
Purkinje layer	3	bc
Granular layer	3	a

This table gives a semiquantitative evaluation of β2-LI based on the number of positive cells (density) and the intensity of immunolabeling. In order to avoid saturation of the signal due to Ni intensification, the assessment of the relative intensity of staining was performed on experiments revealed by DAB (without Ni intensification) or DAB/Ni at several dilutions of the primary antibody.

[a] Density scale: 1 (scattered positive cells), 2 (several positive cells), and 3 (most cells are positive).

[b] Intensity scale: a (weak staining), b (intermediate staining), and c (intense staining).

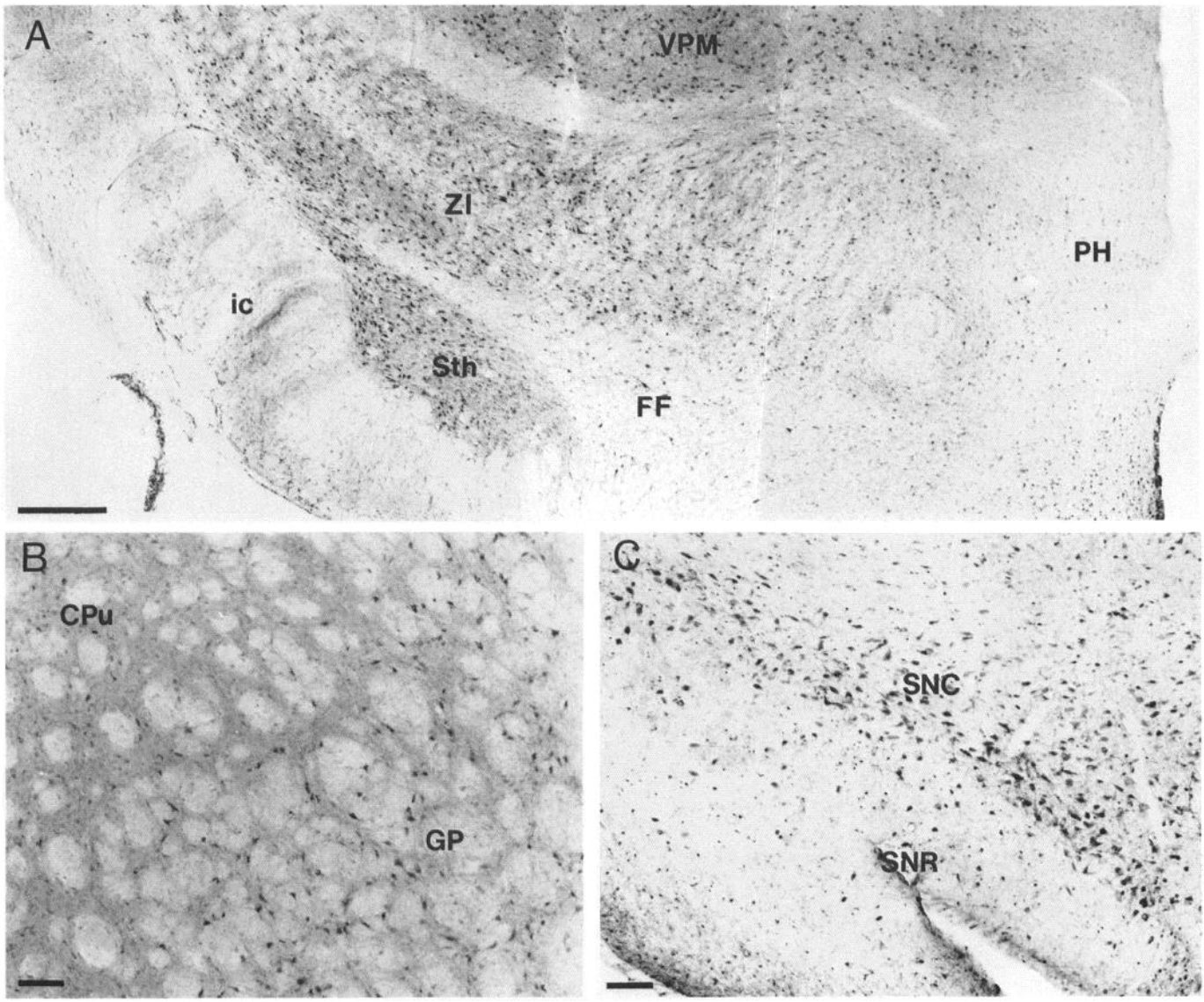

Figure 9. Photomicrographs of β2-LI in rat basal ganglia. *A*, Subthalamic nucleus and adjacent regions. *FF*, fields of Forel; *ic*, internal capsule; *PH*, posterior hypothalamic nucleus; *Sth*, subthalamic nucleus; *VPM*, ventroposterior thalamic nucleus, medial part; *ZI*, zona incerta. Level = bregma −3.8 mm. *B*, Basal ganglia. *CPu*, caudate-putamen; *GP*, globus pallidus. Level = bregma −0.8 mm. *C*, Substantia nigra. *SNC*, substantia nigra, pars compacta; *SNR*, substantia nigra, pars reticulata. Level = bregma −4.8 mm. For *A* and *C*, Ab170 diluted 1:1000; revealed by DAB/Ni. For *B*, Ab170 was diluted 1:500 and revealed by immunogold. Scale bars: *A*, 300 μm; *B* and *C*, 100 μm.

in Purkinje cells and a diffuse signal was observed in the granule cell layer (Fig. 14*A,C*). Again, this pattern corresponds closely with the pattern of β2-LI labeling observed by immunocytochemistry (ICC) (Fig. 14*B,D*).

In order to analyze further the relationship between β2 gene expression and β2-LI, we performed a semiquantitative evaluation of β2-LI and compared this estimation with previous ISH data (Wada et al., 1989). β2-LI was quantified (Table 1) based on the number of positive cells (scale of 0–3) and the intensity of staining (scale of 0–3). The final value corresponds to the sum of these parameters minus 1.5 (to correct for the minimum possible value for the ISH; Wada et al., 1989). Values were assigned to the ISH data as follows: (+) = 0.5, + = 1.0, +(+) = 1.5, etc. Linear regression (Snedecor and Cochran, 1967) revealed a coefficient of correlation of 0.867 ($n = 108$, $p < 0.001$) between the ICC and ISH data. The correlation between β2-LI and β2 mRNA content was highly significant even though the two experimental approaches are very different. Some disparities between ICC and ISH staining patterns were observed, however, at the level of cellular content of β2-LI and β2 mRNA, essentially limited to areas with scattered neurons intensely stained by β2 antibody. For example, measurements in globus pallidus where strong immunostaining was detected in the sparsely distributed pallidal neurons, fulfilled criteria for a high score for ICC (3.5 on our semiquantitative scale) and a low score for ISH (0.5 on our semiquantitative scale). Thus, in spite of the methodological differences between ICC and ISH, the correspondence between β2-LI and the pattern of β2 transcript expression was excellent.

Subcellular distribution at optic level

Detection of β2-LI was restricted to discrete populations of neurons in the CNS. Of interest was the preponderance of cytoplasmic β2-LI observed at the optic level in many areas of

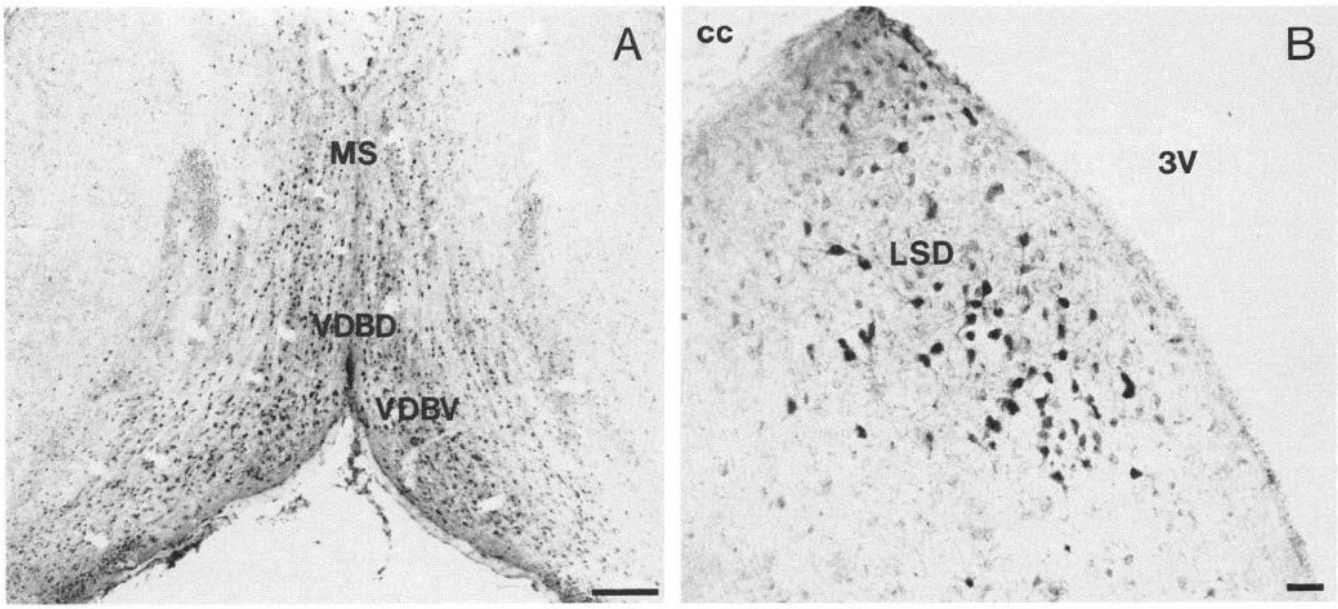

Figure 10. Photomicrographs of β2-LI in rat septal region. *A*, Medial septum. *MS*, medial septum; *VDBD*, nucleus of the vertical limb of the diagonal band, dorsal part; *VDBV*, nucleus of the vertical limb of the diagonal band, ventral part. Level = bregma +1.2 mm; Ab170 diluted 1:1000; revealed by DAB/Ni. *B*, Lateral septum. *cc*, corpus callosum; *LSD*, laterodorsal septum; *3V*, third ventricle. Level = bregma +0.7 mm; Ab170 diluted 1:1000; revealed by immunogold. Scale bars: *A*, 200 μm; *B*, 50 μm.

the brain (see, e.g., Figs. 10*B*, 11*D*, 14*D*). Interpreted to represent β2-containing AChR during the course of biosynthesis and transport to target sites, similar cytoplasmic localization was observed at the ultrastructural level (see below). At the same time, β2-LI in densely packed neuropil was very often seen in various brain regions, indicating that β2-LI exists in nerve processes and terminals (see, e.g., Figs. 2; 8*A,B*; 9*A*; 11*D*).

Not infrequently, neuronal cell nuclei labeled positive for β2-LI (see, e.g., Figs. 8*B*, 10*B, 11D*). In the same experiment, positive cells with positive and negative nuclei were found. Observed in all areas of the brain, this issue remains puzzling. It is important to note, however, that positive nuclei were present exclusively in positive neurons. Under no circumstance did we observe positive nuclei in an otherwise negative cell (except after glutaraldehyde fixation, a procedure known to favor nonspecific nuclear labeling). Similar nuclear staining in positive cells was observed in hippocampal and cortical neurons in primary culture (J. A. Hill, M. Zoli, J.-P. Bourgeois, and J.-P. Changeux, unpublished observations).

Electron microscopy

In an effort to account for the cytoplasmic component of β2-LI and to characterize β2-LI in neuropil, an examination at the ultrastructural level was performed (Fig. 15). All electron microscopic experiments were performed using antiserum 170 (anti-β2 cytoplasmic fusion protein), either purified on an antigen column or conditioned (preadsorbed against DHFR, *Torpedo* AChR, and rat brain acetone powder). Using the immunoperoxidase method, many (though not all) dendritic processes were positive for β2-LI in neuropil of layer III of cerebral cortex (Fig. 15*A*). In layer V cell bodies, DAB/H_2O_2 reaction product deposition could be observed in the cytoplasm in the vicinity of endoplasmic reticulum (ER) (Fig. 15*C*). As expected for an antibody directed against a cytoplasmic epitope, labeling was localized to the cytoplasmic face of ER cisternae. Decoration of ER membranes was heterogeneous, as some segments of reticulum were not stained. Interestingly, labeling of Golgi saccules or vesicles was never observed.

To refine the localization provided by immunoperoxidase, we turned to silver-amplified immunogold detection. Though less sensitive than peroxidase, immunogold labeling provides exquisite detail concerning the ultrastructural topography of antibody binding. This is particularly true given our purpose to localize β2-LI to specific cell membranes, as the DAB/H_2O_2 reaction product may diffuse somewhat before precipitation.

In cortical neuropil, silver grains were associated with the plasma membranes of dendrites and synaptic boutons (Fig. 15*B*). Yet, we rarely observed dense immunoreaction at synaptic profiles using both pre- and postembedding procedures. At present, we cannot explain this dearth of synaptic immunostaining. Among several possibilities, we may postulate steric hindrance effects stemming from the subsynaptic density. Alternatively, it remains a possibility that β2-subunit is not present at the synapse, but rather subserves nonsynaptic neurotransmission (Umbriaco et al., 1991). Experiments using low-temperature resins and cryoultramicrotomy are underway to test whether poor antibody penetration hinders localization of β2-LI at synapses.

In pyramidal cell bodies, DAB/H_2O_2 reaction product (Fig. 15*C*) and silver grain deposition (Fig. 15*D*) were observed associated with the cytoplasmic face of ER membranes. Again, no immunolabeling was seen inside ER cisternae or over Golgi membranes. Consistent with our optic microscopic observations, silver grains were often seen over the nucleus. As before, nuclear localization of reaction product was observed only in positive neurons and in the absence of glutaraldehyde fixation.

Discussion

In the present study, we report the immunohistochemical localization of a neuronal AChR resolved at the level of a subunit protein. To this end, we developed specific antisera directed

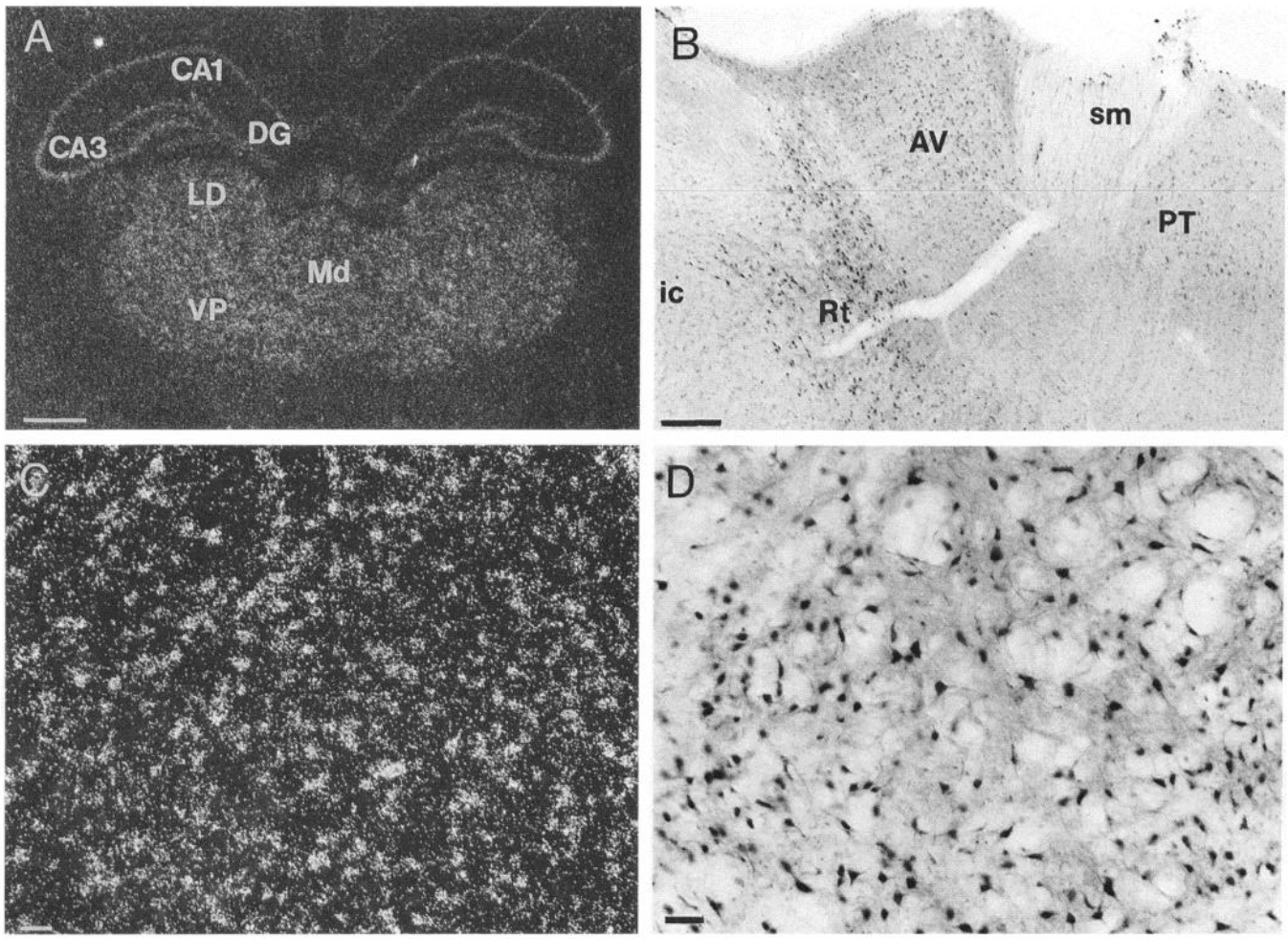

Figure 11. Photomicrographs of β2-LI and dark-field ISH images of β2 mRNA in rat thalamus. *A*, Film autoradiogram of β2 transcript localization in thalamic and hippocampal regions. Same oligonucleotide as in Figure 4. *CA1* and *CA3*, hippocampal fields CA1 and CA3; *DG*, dentate gyrus; *LD*, laterodorsal thalamic nucleus; *VP*, ventroposterior thalamic nuclei; *Md*, midline thalamic nuclei. Level = bregma −3.3 mm. *B*, Anterior thalamus. *AV*, anteroventral thalamic nucleus; *PT*, paratenial thalamic nucleus; *sm*, stria medullaris; *Rt*, reticular thalamic nucleus; *ic*, internal capsule. Level = bregma −1.3 mm; Ab170 diluted 1:1000; revealed by DAB/Ni. *C*, Emulsion autoradiogram of β2 ISH in ventroposterior thalamic nucleus, medial part. Level = bregma −2.8 mm. *D*, β2-LI in ventroposterior thalamic nucleus, medial part, revealed by DAB/Ni. Level = bregma −2.8 mm. Scale bars: *A*, 1 mm; *B*, 200 μm; *C* and *D*, 50 μm.

against unique regions of the β2-subunit primary structure and have examined the distribution of AChR β2-subunit protein in rat brain at the tissue, cell, and ultrastructural levels. Specificity of the immunostaining was assured by several means, the most powerful being anatomic controls using antibodies directed against multiple regions of the β2 protein molecule. Indeed, special measures were undertaken to ensure a specific labeling pattern as the β2-subunit is part of a family of homologous membrane proteins. Accumulated evidence derived from a variety of sources indicate that our reported β2-LI pattern very likely reveals the localization of β2-subunit.

For practical reasons, it is difficult to compare our pattern of β2-LI with previous morphological studies. Overall, however, the distribution of β2-LI broadly parallels that of ^{3}H-nicotine binding sites in the brain (Clarke et al., 1985), being strong in the thalamus, intermediate in striatum and cortex, and weak in hypothalamus. On the other hand, the β2-LI staining pattern markedly differs from the distribution of ^{125}I-α-bungarotoxin binding in rat brain (Clarke et al., 1985), which is intense in the hypothalamus and weak in thalamus and striatum.

With a few notable exceptions, immunohistochemical staining using cross-reacting antibodies raised against *Torpedo* AChR parallels β2-LI. A monoclonal antibody directed against the main immunogenic region (MIR) of *Torpedo* AChR, however, does not label magnocellular cholinergic cell groups of the basal forebrain (Deutch et al., 1987), a locus of intense β2-LI. A second monoclonal antibody raised against *Torpedo* AChR α-subunit labels all six layers of rat cortex, the Golgi apparatus of cortical neurons, and postsynaptic membranes, but does not stain axons (Schröder et al., 1989), a pattern distinct from that of β2-LI. Immunolabeling in rat brain using mAb270 revealed a pattern similar to the nerve terminal portion of our β2-LI staining (Swanson et al., 1987). This monoclonal antibody, raised against AChR immunopurified from chicken, recognizes denatured β2 in *in vitro* assays (Whiting and Lindstrom, 1987). Differences in affinity for somatic versus terminal antigen may account for these dissimilarities. Alternatively, signal saturation using radioactively labeled antibody (Swanson et al., 1987) would emphasize background neuropil staining relative to cytoplasmic staining.

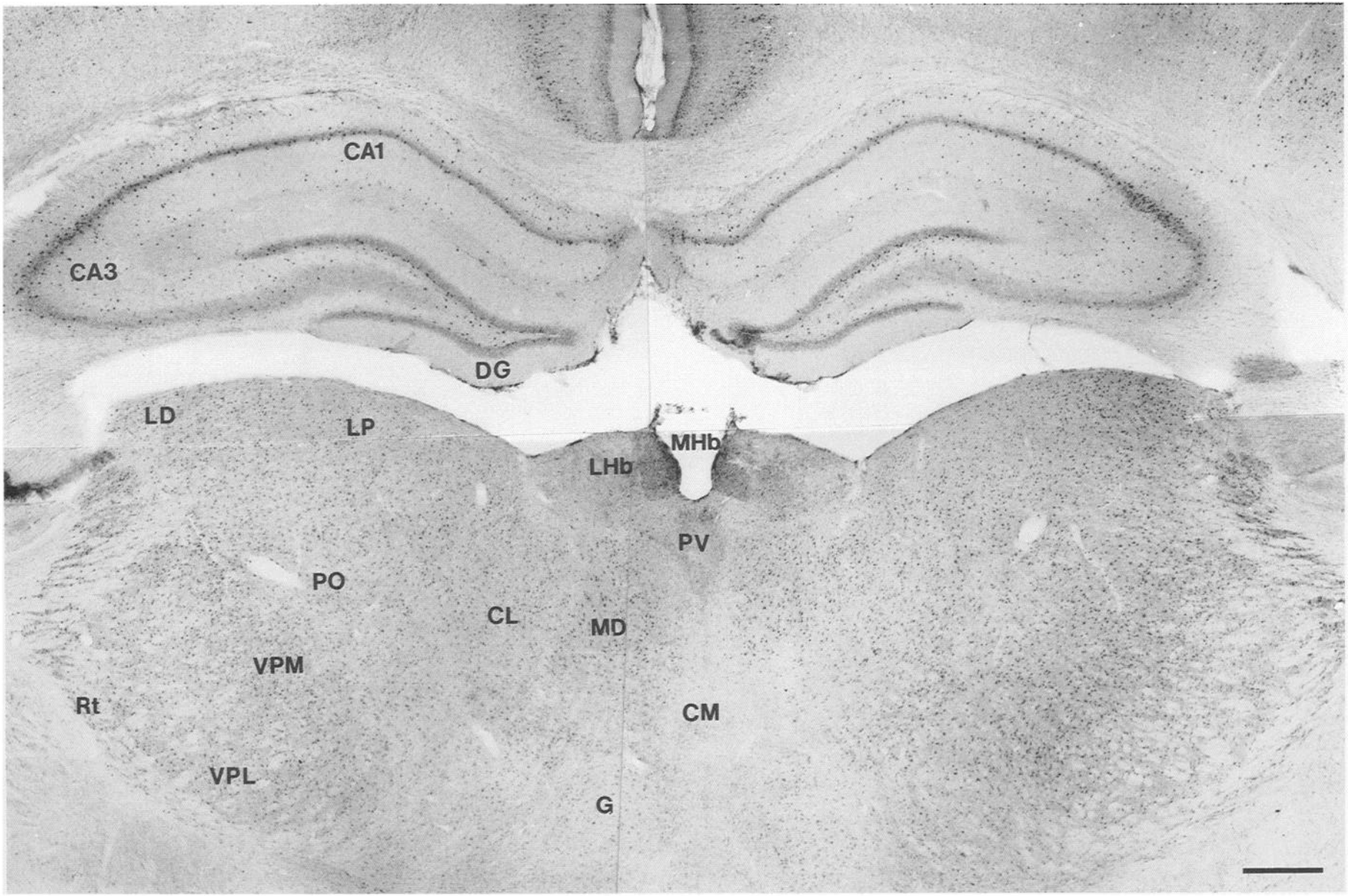

Figure 12. Photomicrograph of β2-LI in rat thalamic and hippocampal regions. *CA1* and *CA3*, hippocampal fields CA1 and CA3; *CL*, centrolateral thalamic nucleus; *CM*, centromedial thalamic nucleus; *DG*, dentate gyrus; *G*, nucleus gelatinosus; *LD*, laterodorsal thalamic nucleus; *LHb*, lateral habenula; *LP*, lateroposterior thalamic nucleus; *MD*, mediodorsal thalamic nucleus; *MHb*, medial habenula; *PO*, posterior thalamic nuclear group; *PV*, paraventricular thalamic nucleus; *Rt*, reticular thalamic nucleus; *VPL*, ventroposterior thalamic nucleus, lateral part; *VPM*, ventroposterior thalamic nucleus, medial part. Level = bregma −3.0 mm; Ab170 diluted 1:1000; revealed by DAB/Ni. Scale bar, 500 μm.

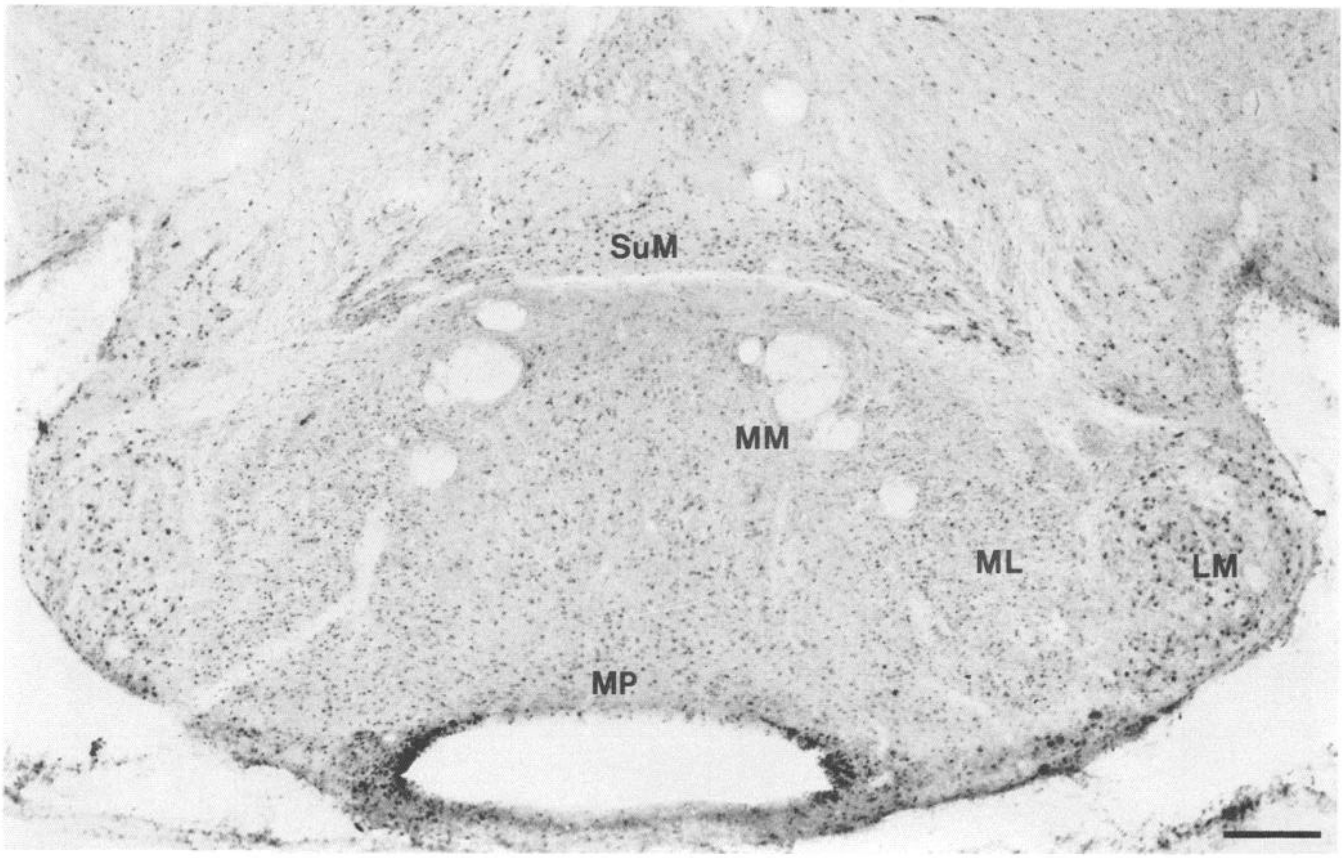

Figure 13. Photomicrographs of β2-LI in rat mammillary bodies. *LM*, lateral mammillary nucleus; *ML*, medial mammillary nucleus, lateral part; *MM*, medial mammillary nucleus, medial part; *MP*, medial mammillary nucleus, posterior part; *SuM*, supramammillary nucleus. Level = bregma −4.8 mm; Ab170 diluted 1:1000; revealed by DAB/Ni. Scale bar, 200 μm.

The distribution of β2-LI in cell bodies closely resembles the distribution of β2 transcript in the brain. This is true, based both on qualitative evaluation and semiquantitative regional comparison, despite prominent methodological differences between these two approaches. β2-LI was quantified (Table 1) based on the number of positive cells and the intensity of staining. Linear regression revealed a coefficient of correlation of 0.867 between the ICC and ISH data. This striking correlation confirms that our pattern of β2-LI staining in cell bodies corresponds more closely to the pattern of β2 gene expression than it does to previously reported efforts to map AChR in the brain.

Comparing our immunostaining pattern with previously published cholinergic markers, we observed an impressive correspondence between the distribution of β2-LI and that of AChE (Butcher and Woolf, 1984). The widespread distribution of AChE has led investigators to regard it as a nonspecific marker of central cholinergic systems (Lehmann and Fibiger, 1979). Indeed, nicotinic transmission has been held to represent a relatively minor component of neuronal signaling in the CNS, and the diffuse distribution of AChE is thought to reflect the more widespread role of muscarinic mechanisms (e.g., Krnjevic, 1988). Thus, present data suggest that, as is the case at the neuromuscular junction (Bevan and Steinbach, 1977), AChE colocalizes with nicotinic receptors in the CNS over the greater part of its distribution.

A precedent exists for the strong cytoplasmic signal we observe with β2 subunit antisera. In ciliary and choroid cells of chick ciliary ganglia, prevalent intracellular staining has been reported using an anti-MIR monoclonal antibody (Jacob et al., 1986; Jacob, 1991). Similarly, antibodies directed against *Torpedo* AChR stain neuronal perikarya in brain (Deutch et al., 1987; Schröder et al., 1989). Among other members of the ligand-gated ion channel superfamily, $GABA_A$ receptors accumulate in the somata of GABAergic stellate and basket cells of cerebellum (Somogyi et al., 1989), and glutamate receptor GluR1 subunits collect in cerebellar Purkinje cells (Rogers et al., 1991). L-type calcium channels accumulate intracellularly in hippocampal pyramidal neurons (Westenbroek et al., 1990), and in neonatal rat brain, a significant intracellular pool of sodium channel α-subunit has been detected (Schmidt et al., 1985). Muscle-type AChR in myotubes and in BC3H1 cells exist in both plasmalemmal and internal pools (Devreotes et al., 1977; Pestronk, 1985). Indeed, a substantial proportion of the cellular AChR content is stored intracellularly or degraded without ever reaching the cell surface of muscle (Merlie and Lindstrom, 1983; Merlie, 1984) and cultured ciliary ganglion neurons (Stollberg and Berg, 1987). Thus, existence of an intracellular pool of protein seems to be a common feature among ion channels (but cf. glycine receptor, Triller et al., 1985). This cytoplasmic store of protein may correspond to improperly assembled "abortive" multisubunit complexes; alternatively, it may represent a readily accessible reserve of receptor in case of developmental contingencies (Jacob et al., 1986).

We have observed strong staining of neuronal ER cisternae

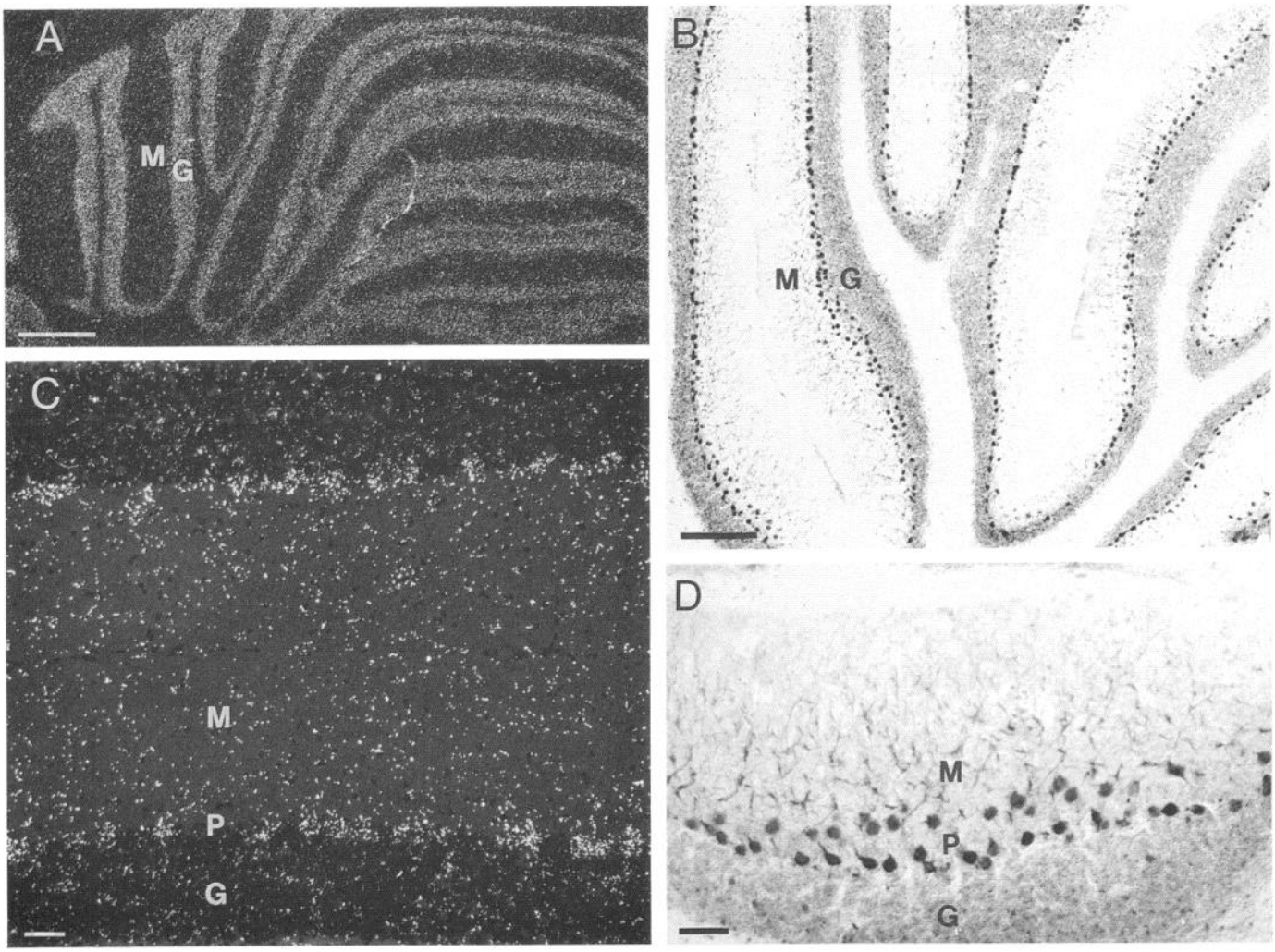

Figure 14. Photomicrographs of β2-LI and dark-field ISH images of β2 mRNA in rat cerebellum. *A*, Film autoradiogram of β2 transcript localization in cerebellum. Same oligonucleotide as in Figure 4. *B*, β2-LI in cerebellum. Ab170 diluted 1:1000; revealed by DAB/Ni. *C*, Emulsion autoradiogram of β2 ISH in cerebellar cortex. Note that toluidine blue counterstaining of densely packed granule cells partially masks the diffuse specific signal present over these cells (see *A*). *D*, β2-LI in cerebellar cortex, revealed by DAB/Ni. In all panels, level = bregma −10.3 mm. *G*, granular layer; *M*, molecular layer; *P*, Purkinje cell layer. Scale bars: *A*, 1 mm; *B*, 250 μm; *C* and *D*, 50 μm.

but failed to detect immunoprecipitate over Golgi membranes, suggesting that β2-containing AChR accumulates in the ER during the course of biosynthesis and assembly. Similarly, in ciliary ganglion neurons, a predominance of anti-MIR binding sites localized to ER relative to Golgi was reported (Jacob et al., 1986; Jacob, 1991). Upon heterologous expression in fibroblasts, *Torpedo* AChR subunits assemble in the ER and pass rapidly through the Golgi to the plasma membrane (Ross et al., 1991). Together, these observations lend support to the notion that the rate-limiting steps in AChR biosynthesis occur in the ER comprising amino acid polymerization, conformation maturation of individual subunits, and possibly macromolecular assembly (Merlie, 1984); once signals for receptor sorting and targeting are received, AChR passes rapidly through the Golgi apparatus and is transported to the plasmalemma.

In agreement with the *in situ* localization of β2 transcript in rat (Wada et al., 1989; present data) and chick (Morris et al., 1990), we observed β2-LI widely distributed throughout the brain, further supporting the notion of the global character of nicotinic circuitry. This, combined with the strong cytoplasmic component of labeling, suggests that β2 is available to be incorporated into AChRs in many regions of the nervous system. The structural β-subunit of the inhibitory glycine receptor is also widely expressed in rat brain relative to ligand-binding subunits (Fujita et al., 1991; Malosio et al., 1991). These data imply that an important mechanism underlying AChR heterogeneity may reside in the regulation of α-subunit biosynthesis; the control of β2 expression is relatively unrestricted. Non-ligand-binding subunits may function in a multimodal fashion, subserving generalized structural capacities upon assembly with different α-subunits.

In several brain regions including the hippocampal molecular layer, striatum, ventral posterior thalamus, and entopeduncular and subthalamic nuclei, we observed a fine and diffuse staining that can be interpreted to be staining of nerve terminal fields. Other data indicate that AChRs undergo dendritic and axonal transport in the brain (e.g., Swanson et al., 1987; Mulle et al., 1991). Thus, it may be inferred that axonal and dendritic transport pathways mediate AChR trafficking in individual neurons.

The physiologic role of nicotinic transmission in the brain is

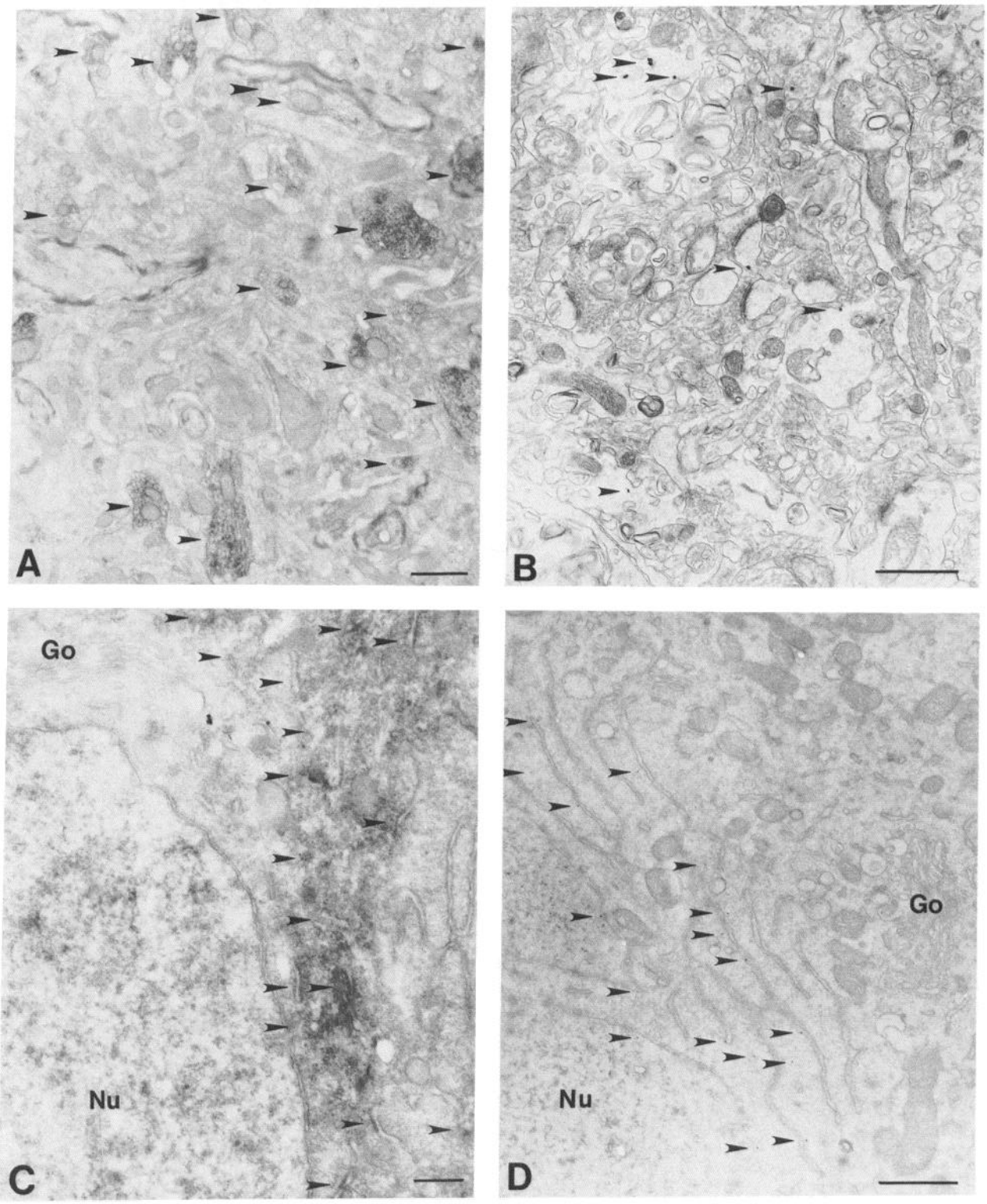

Figure 15. Distribution of β2-like immunolabeling (anti-β2 cytoplasmic fusion protein) in rat frontoparietal cortex (neuropil in layer III, somata in layer V). *A*, Distinct labeling of some dendrites (*arrowheads*) as revealed by deposition of the DAB/H_2O_2 reaction product in cortical neuropil. *B*, Immunogold staining reveals silver grains localized to the cytoplasmic face of the dendritic plasma membrane. *C*, Immunoperoxidase labeling of the perikaryon of a pyramidal cell. Note that DAB/H_2O_2 reaction product is associated with the ER, localized to the cytoplasmic face (*arrowheads*). *D*, The higher resolution afforded by the immunogold reaction reveals localization to the cytoplasmic surface of ER membrane. Occasional grains were observed over the nucleus (*Nu*) but few over the Golgi apparatus (*Go*). Images are of unstained, ultrathin sections. Scale bars, 1 μm.

not well characterized. However, perturbed nicotinic mechanisms may underlie certain disease states. For example, it has been reported that the nucleus basalis of Meynert and the nucleus of the diagonal band are selectively impoverished of their magnocellular neurons in Alzheimer's disease patients (Davies and Maloney, 1976; Whitehouse et al., 1982; Yankner and Mesulam, 1991). These neurons, which stain intensely for β2-LI, are the major source of cortical afferentation employing ACh. Further studies of the neuronal biosynthesis and transport of AChR subunits should help elucidate the function of nicotinic transmission in the brain.

References

Anand R, Conroy WG, Schoepfer R, Whiting P, Lindstrom P (1991) Neuronal nicotinic acetylcholine receptors expressed in *Xenopus* oocytes have a pentameric quaternary structure. J Biol Chem 266:11192–11198.

Bevan S, Steinbach JH (1977) The distribution of α-bungarotoxin binding sites on mammalian skeletal muscle developing *in vivo*. J Physiol (Lond) 267:195–213.

Bossy B, Ballivet M, Spierer P (1988) Conservation of neural nicotinic acetylcholine receptors from *Drosophila* to vertebrate central nervous systems. EMBO J 7:611–618.

Boulter J, Evans K, Goldman D, Martin G, Treco D, Heinemann S, Patrick J (1986) Isolation of a cDNA clone coding for a possible neural nicotinic acetylcholine receptor α-subunit. Nature 319:368–374.

Boulter J, O'Shea-Greenfield A, Duvoisin RM, Connolly JG, Wada E, Jensen A, Gardner PD, Ballivet M, Deneris ES, McKinnon D, Heinemann S, Patrick J (1990) α3, α5, and β4: three members of the rat neuronal nicotinic acetylcholine receptor-related gene family form a gene cluster. J Biol Chem 265:4472–4482.

Butcher LL, Woolf NJ (1984) Histochemical localization of acetylcholinesterase in the central nervous system: clues to the localization of cholinergic neurons. In: Handbook of chemical neuroanatomy, Vol 3, Classical transmitters and transmitter receptors in the CNS, Pt II, pp 1–50. Amsterdam: Elsevier.

Cauley K, Agranoff BW, Goldman D (1989) Identification of a novel nicotinic acetylcholine receptor structural subunit expressed in goldfish retina. J Cell Biol 108:637–645.

Cauley K, Agranoff BW, Goldman D (1990) Multiple nicotinic acetylcholine receptor genes are expressed in goldfish retina and tectum. J Neurosci 10:670–683.

Changeux JP, Babinet C, Bessereau J-L, Bessis A, Cartaud J, Daubas P, Devillers-Thiéry A, Duclert A, Hill JA, Jasmin B, Klarsfeld A, Laufer R, Nghiêm H-O, Piette J, Roa M, Salmon AM (1990) Compartmentalization of acetylcholine receptor gene expression during development of the neuromuscular junction. Cold Spring Harbor Symp Quant Biol 55:381–406.

Clarke PBS, Schwartz RD, Paul SM, Pert CB, Pert A (1985) Nicotinic binding in rat brain: autoradiographic comparison of [^{3}H]acetylcholine, [^{3}H]nicotine, and [^{125}I]α-bungarotoxin. J Neurosci 5:1307–1315.

Cooper E, Couturier S, Ballivet M (1991) Pentameric structure and subunit stoichiometry of a neuronal nicotinic acetylcholine receptor. Nature 350:235–238.

Couturier S, Bertrand D, Matter J-M, Hernandez M-C, Bertrand S, Millar N, Valera S, Barkas T, Ballivet M (1990) A neural nicotinic acetylcholine receptor subunit (α7) is developmentally regulated and forms a homo-oligomeric channel blocked by α-btx. Neuron 5:847–856.

Daubas P, Devillers-Thiéry A, Geoffroy B, Martinez S, Bessis A, Changeux J-P (1990) Differential expression of the neuronal acetylcholine receptor α2 subunit gene during chick brain development. Neuron 5:49–60.

Davies P, Maloney AJF (1976) Selective loss of central cholinergic neurons in Alzheimer's disease. Lancet 2:1403.

Deneris ES, Connolly J, Boulter J, Wada E, Wada K, Swanson LW, Patrick J, Heinemann S (1988) Primary structure and expression of β2: a novel subunit of neuronal nicotinic acetylcholine receptors. Neuron 1:45–54.

Deneris ES, Boulter J, Swanson LW, Patrick J, Heinemann S (1989) β3: a new member of nicotinic acetylcholine receptor gene family is expressed in brain. J Biol Chem 264:6268–6272.

Deutch AY, Holliday J, Roth RH, Chun LLY, Hawrot E (1987) Immunohistochemical localization of a neuronal nicotinic acetylcholine receptor in mammalian brain. Proc Natl Acad Sci USA 84:8697–8701.

Devreotes PN, Gardner JM, Fambrough DM (1977) Kinetics of biosynthesis of acetylcholine receptor and subsequent incorporation into plasma membrane of cultured chick skeletal muscle. Cell 10:365–373.

Duvoisin RM, Deneris ES, Patrick J, Heinemann S (1989) The functional diversity of the neuronal nicotinic acetylcholine receptors is increased by a novel subunit: β4. Neuron 3:487–496.

Fujita M, Sato K, Sato M, Inoue T, Kozuka T, Tohyama M (1991) Regional distribution of the cells expressing glycine receptor β subunit mRNA in the rat brain. Brain Res 560:23–37.

Goldman D, Deneris E, Luyten W, Kochhar A, Patrick J, Heinemann J (1987) Members of a nicotinic acetylcholine receptor gene family are expressed in different regions of the mammalian central nervous system. Cell 48:965–973.

Gottesman S, Halpern E, Trisler P (1981) Role of sulA and sulB in filamentation by lon mutants of *Escherichia coli* K-12. J Bacteriol 148:265–273.

Harlow E, Lane D (1988) Antibodies: a laboratory manual, pp 86–87. Cold Spring Harbor, NY: Cold Spring Harbor Laboratory.

Hermans-Borgmeyer I, Zopf D, Ryseck R-P, Hovemann B, Betz H, Gundelfinger ED (1986) Primary structure of a developmentally regulated nicotinic acetylcholine receptor protein from *Drosophila*. EMBO J 5:1503–1508.

Hill JA, Nghiêm H-O, Changeux J-P (1991) Serine-specific phosphorylation of nicotinic receptor-associated 43K protein. Biochemistry 30:5579–5585.

Hökfelt T (1991) Neuropeptides in perspective: the last ten years. Neuron 7:867–879.

Isenberg KE, Meyer GE (1989) Cloning of a putative neuronal nicotinic acetylcholine receptor subunit. J Neurochem 52:988–991.

Jacob MH (1991) Acetylcholine receptor expression in developing chick ciliary ganglion neurons. J Neurosci 11:1701–1712.

Jacob MH, Lindstrom JM, Berg DK (1986) Surface and intracellular distribution of a putative neuronal nicotinic acetylcholine receptor. J Cell Biol 103:205–214.

Krnjevic K (1988) Central cholinergic transmission: the physiological evidence. In: Handbook of experimental pharmacology, Vol 86, The cholinergic synapse, pp 633–662. Berlin: Springer.

Lehmann JC, Fibiger HC (1979) Acetylcholinesterase and the cholinergic neuron. Life Sci 25:1939–1947.

Luetje CW, Patrick J (1991) Both α- and β-subunits contribute to the agonist sensitivity of neuronal nicotinic acetylcholine receptors. J Neurosci 11:837–845.

Malosio M-L, Marquèze-Pouey B, Kuhse J, Betz H (1991) Widespread expression of glycine receptor subunit mRNAs in the adult and developing rat brain. EMBO J 10:2401–2409.

Marshall J, Buckingham SD, Shingai R, Lunt GG, Goosey MW, Darlison MG, Sattelle DB, Barnard EA (1990) Sequence and functional expression of a single α subunit of an insect nicotinic acetylcholine receptor. EMBO J 9:4391–4398.

Merlie JP (1984) Biogenesis of the acetylcholine receptor, a multisubunit integral membrane protein. Cell 36:573–575.

Merlie JP, Lindstrom J (1983) Assembly *in vivo* of mouse muscle acetylcholine receptor: identification of an alpha subunit species that may be an assembly intermediate. Cell 34:747–757.

Morris BJ, Hicks AA, Wisden W, Darlison MG, Hunt SP, Barnard EA (1990) Distinct regional expression of nicotinic acetylcholine receptor genes in chick brain. Mol Brain Res 7:305–315.

Mulle C, Vidal C, Benoit P, Changeux J-P (1991) Existence of different subtypes of nicotinic acetylcholine receptors in the rat habenulo-interpeduncular system. J Neurosci 11:2588–2597.

Nef P, Oneyser C, Alliod C, Couturier S, Ballivet M (1988) Genes expressed in the brain define three distinct neuronal nicotinic acetylcholine receptors. EMBO J 7:595–601.

Paxinos G, Watson C (1982) The rat brain in stereotaxic coordinates. New York: Academic

Pestronk A (1985) Intracellular acetylcholine receptors in skeletal muscles of the adult rat. J Neurosci 5:1111–1117.

Rogers SW, Hughes TE, Hollmann M, Gasic GP, Deneris ES, Heinemann S (1991) The characterization and localization of the gluta-

mate receptor subunit GluR1 in the rat brain. J Neurosci 11:2713–2724.

Ross AF, Green WN, Hartman DS, Claudio T (1991) Efficiency of acetylcholine receptor subunit assembly and its regulation by cAMP. J Cell Biol 113:623–636.

Sambrook J, Fritsch EF, Maniatis T (1989) Molecular cloning: a laboratory manual. Cold Spring Harbor, NY: Cold Spring Harbor Laboratory.

Sawruk E, Schloss P, Betz H, Schmitt B (1990) Heterogeneity of *Drosophila* nicotinic acetylcholine receptors: SAD, a novel developmentally regulated α-subunit. EMBO J 9:2671–2677.

Schmidt J, Rossie S, Catterall WA (1985) A large intracellular pool of inactive Na channel alpha subunits in developing rat brain. Proc Natl Acad Sci USA 82:4847–4851.

Schoepfer R, Whiting P, Esch F, Blacher R, Shimasaki S, Lindstrom J (1988) cDNA clones coding for the structural subunit of a chicken brain nicotinic acetylcholine receptor. Neuron 1:241–248.

Schoepfer R, Conroy WG, Whiting P, Gore M, Lindstrom J (1990) Brain α-bungarotoxin binding protein cDNAs and mAbs reveal subtypes of this branch of the ligand-gated ion channel gene superfamily. Neuron 5:35–48.

Schröder H, Zilles K, Maelicke A, Hajós F (1989) Immunohisto- and cytochemical localization of cortical nicotinic cholinoceptors in rat and man. Brain Res 502:287–295.

Snedecor GW, Cochran WG (1967) Statistical methods. Ames: Iowa State University.

Somogyi P, Takagi H, Richards JG, Mohler H (1989) Subcellular localization of benzodiazepine/$GABA_A$ receptors in the cerebellum of rat, cat, and monkey using monoclonal antibodies. J Neurosci 9:2197–2209.

Stollberg J, Berg DK (1987) Neuronal acetylcholine receptors: fate of surface and internal pools in cell culture. J Neurosci 7:1809–1815.

Stüber D, Matile H, Garotta G (1990) System for high-level production in *Escherichia coli* and rapid purification of recombinant proteins: application to epitope mapping, preparation of antibodies, and structure-function analysis. Immunol Methods 4:121–152.

Swanson LW, Simmons DM, Whiting PJ, Lindstrom J (1987) Immunohistochemical localization of neuronal nicotinic receptors in the rodent central nervous system. J Neurosci 7:3334–3342.

Triller A, Cluzeaud F, Pfeiffer F, Betz H, Korn H (1985) Distribution of glycine receptors at central synapses: an immunoelectron microscopy study. J Cell Biol 101:683–688.

Umbriaco D, Watkins KC, Descarries L, Cozzari C, Hartman B (1991) Non-junctional cholinergic (ACh) innervation of adult rat parietal cortex. Third IBRO World Congress of Neuroscience, Montreal, abstract P54.2.

Wada E, Wada K, Boulter J, Deneris E, Heinemann S, Patrick J, Swanson LW (1989) Distribution of alpha2, alpha3, alpha4, and beta2 neuronal nicotinic receptor subunit mRNAs in the central nervous system: a hybridization histochemical study in the rat. J Comp Neurol 284:314–335.

Wada E, McKinnon D, Heinemann S, Patrick J, Swanson LW (1990) The distribution of mRNA encoded by a new member of the neuronal nicotinic acetylcholine receptor gene family (α5) in the rat central nervous system. Brain Res 526:45–53.

Wada K, Ballivet M, Boulter J, Connolly J, Wada E, Deneris ES, Swanson LW, Heinemann S, Patrick J (1988) Functional expression of a new pharmacological subtype of brain nicotinic acetylcholine receptor. Science 240:330–334.

Wadsworth SC, Rosenthal LS, Kammermeyer KL, Potter MB, Nelson DJ (1988) Expression of a *Drosophila* melanogaster acetylcholine receptor-related gene in the central nervous system. Mol Cell Biol 8:778–785.

Westenbroek RE, Ahlijanian MK, Catterall WA (1990) Clustering of L-type Ca^{2+} channels at the base of major dendrites in hippocampal pyramidal neurons. Nature 347:281–284.

Whitehouse PJ, Price DL, Struble RG, Clark AW, Coyle JT, DeLong MR (1982) Alzheimer's disease and senile dementia: loss of neurons in the basal forebrain. Science 215:1237–1239.

Whiting P, Lindstrom J (1987) Purification and characterization of a nicotinic acetylcholine receptor from rat brain. Proc Natl Acad Sci USA 84:595–599.

Yankner BA, Mesulam M-M (1991) β-amyloid and the pathogenesis of Alzheimer's disease. New Engl J Med 325:1849–1857.

Young WS (1989) *In situ* hybridization histochemistry. In: Handbook of chemical neuroanatomy, Vol 8, Analysis of neuronal microcircuits and synaptic interactions, pp 481–512. Amsterdam: Elsevier.